



# **Autonomous Modeling of a 3D Environment with Drones**

Masterarbeit

zur Erlangung des akademischen Grades  
**Master of Science in Engineering (M.Sc.)**

Eingereicht bei:

**Fachhochschule Kufstein Tirol Bildungs GmbH**  
**Data Science & Intelligent Analytics**

Verfasser/in:

**Julian Bialas, BSc**

**1910837917**

Erstgutachter : Prof. (FH) PD Dr. Mario Döller  
Zweitgutachter : Robert Kathrein, MSc

Abgabedatum:

**06. July 2020**

# **Eidesstattliche Erklärung**

Ich erkläre hiermit, dass ich die vorliegende Masterarbeit selbstständig und ohne fremde Hilfe verfasst und in der Bearbeitung und Abfassung keine anderen als die angegebenen Quellen oder Hilfsmittel benutzt sowie wörtliche und sinngemäße Zitate als solche gekennzeichnet habe. Die vorliegende Masterarbeit wurde noch nicht anderweitig für Prüfungszwecke vorgelegt.

Kufstein, 06. July 2020

---

Julian Bialas, BSc

# **Sperrvermerk**

Ich habe die Sperrung meiner Masterarbeit beantragt, welche von der Studiengangsleitung genehmigt wurde.

Kufstein, 06. July 2020

---

Julian Bialas, BSc

# Contents

<b>1</b>	<b>Introduction</b>	<b>1</b>
<b>2</b>	<b>Evaluation of the vSLAM Algorithms</b>	<b>5</b>
2.1	Related Work . . . . .	5
2.1.1	Introduction and History of SLAM . . . . .	5
2.1.2	Definitions . . . . .	9
2.1.3	ORB-SLAM . . . . .	11
2.1.4	DSO-SLAM . . . . .	16
2.1.5	DSM-SLAM . . . . .	19
2.2	Evaluation Methods . . . . .	23
2.2.1	Dataset . . . . .	23
2.2.2	Evaluation Criteria . . . . .	24
2.2.3	Setup and Environment . . . . .	29
2.3	Results . . . . .	31
2.3.1	Trajectory Evaluation . . . . .	31

Contents	IV
2.3.2 Pointcloud Evaluation . . . . .	34
2.3.3 Calculation Time . . . . .	38
2.4 Discussion . . . . .	40
2.4.1 Conclusion of SLAM-Algorithm Evaluation . . . . .	40
3 Fully Automated Exploration System	41
3.1 Suggested ROS Framework . . . . .	41
3.1.1 TUM Simulation Node . . . . .	45
3.1.2 ORB-SLAM Node . . . . .	48
3.1.3 Alignment node . . . . .	50
3.1.4 Position Estimation Node . . . . .	56
3.1.5 Transformation and Restriction Node . . . . .	60
3.1.6 Flight Path Planning Node . . . . .	63
3.2 Current setup . . . . .	70
3.2.1 Known Issues . . . . .	72
4 Summary	75

# List of Figures

1	Automated exploration system, based on a SLAM algorithm and a path planning algorithm. . . . .	2
2	Overview of the SLAM concept. Source: [8] . . . . .	6
3	Overview of the system components extracted from [21] . . . . .	11
4	Neighbor pixels considered for the photometric error calculation. Source: [10] . . . . .	17
5	Keyframe and Point Selection of DSM. Source: [37] . . . . .	21
6	Point cloud ground truth of sequence V1_01_easy visualized with python package pptk . . . . .	24
7	Trajectory error after alignment. Source: [36] . . . . .	27
8	Orthogonal projection of a point in the evaluated point cloud ( $\widehat{p_1}$ ) on the planar of the ground truth point cloud. The error $e$ , determines how far the considered point for the ground truth lies from the actual point of the ground truth. . . . .	28

9	Ground truth flight path and evaluated flight path of each algorithm after alignment with the method of Umeyama in the x and y axis in meters. Left the sequence MH01, middle the sequence V102 and right the sequence V203 is displayed. . . . .	32
10	The positional error over time in meters. The vertical lines indicate the beginning of a new sequence . . . . .	33
11	Boxplot of all euclidean distances between the ground truth position of the keyframe and the evaluated position after alignment with the method of Umeyama. Outliers greater than 1.5 are not displayed for clarity reasons. . . . .	35
12	The ground truth of the point cloud from Sequence V101 (white points) and the evaluated points by each algorithm (red points). The points in Figure (a) are twice as large for better visibility (ORB-SLAM generates only few points). . . . .	37
13	Boxplot of the euclidean distances between an evaluated point and the closest point of the ground truth point cloud. For computational feasibility, for each sequence and algorithm, 500 points for evaluation are sampled randomly . . . . .	38
14	Influence of downsizing of the images on the trajectory error (a) and the computation time (b) for the sequence V101. . . . .	40
15	Overview over the suggested ROS framework for the simulated case . . . . .	43
16	Overview over the suggested ROS framework for the real life case	45
17	Tum simulator setup. Source: <a href="http://wiki.ros.org/tum_simulator">http://wiki.ros.org/tum_simulator</a>	46

18	Calculation method for estimation the position in the initialization process in order to find the true scale. . . . .	59
19	The drone in a gazebo simulation in a), the output of the front camera of the drone in b) and the ORB-SLAM algorithm applied on the front camera output in with the detected ORB features marked green c). . . . .	71

## List of Tables

# List of Listings

1	Drone navigation command . . . . .	46
2	Main part of the scale estimation node . . . . .	52
3	Main part of the position estimation node . . . . .	58
4	Adding upper and lower restrictions to point cloud. . . . .	63
5	Launching the simulated environment . . . . .	71
6	Launching different world . . . . .	73

# **List of Acronyms**

**SLAM** Simulatanious Localization and Mapping

**vSLAM** visual SLAM

**ROS** Roboter Operating System

**DSO** Direct Sparse Odometry

**DSM** Direct Sparce Mapping

**ORB** Oriented FAST and Rotated BRIEF

**FH Kufstein Tirol**

**Data Science & Intelligent Analytics**

Abstract of the thesis: **Autonomous Modeling of a 3D Environment with Drones**

**Author:** Julian Bialas, BSc

**First reviewer:** Prof. (FH) PD Dr. Mario Döller

**Second reviewer:** Robert Kathrein, MSc

06. July 2020

**FH Kufstein Tirol**

**Data Science & Intelligent Analytics**

Kurzfassung der Masterarbeit: **Autonomous Modeling of a 3D Environment  
with Drones**

**Verfasser:** Julian Bialas, BSc

**Erstgutachter:** Prof. (FH) PD Dr. Mario Döller

**Zweitgutachter:** Robert Kathrein, MSc

06. July 2020

# 1. Introduction

Multiple applications exist for the autonomous exploration and mapping tasks with drones, such as search and rescue-, inspection- and surveillance operations [34].

The autonomous exploration task can be divided into three subproblems: localization, mapping, and path planning [35]. All three tasks should be performed simultaneously within an environment, which the drone has no information on a priori.

The localization task contains the estimation of the position of the drone within this environment and the mapping task refers to the incremental creation of a 3-dimensional map. Multiple methods exist, that combine these two tasks in a so-called simultaneous localization and mapping (SLAM) algorithm. The development of these SLAM algorithms is one of the most researched topics in the field of robotics [12].

SLAM is used for many applications including mobile robotics, self-driving cars, unmanned aerial vehicles, or autonomous underwater vehicles [7].

When combining a SLAM algorithm with a path planning algorithm, an autonomous exploration system is created. The autonomous exploration using SLAM and a path planning algorithm is sometimes also referred to as active

SLAM [16]. This active SLAM process is displayed in figure 1. Details on how such a system can be initiated and terminated, can be found in section 3.1.

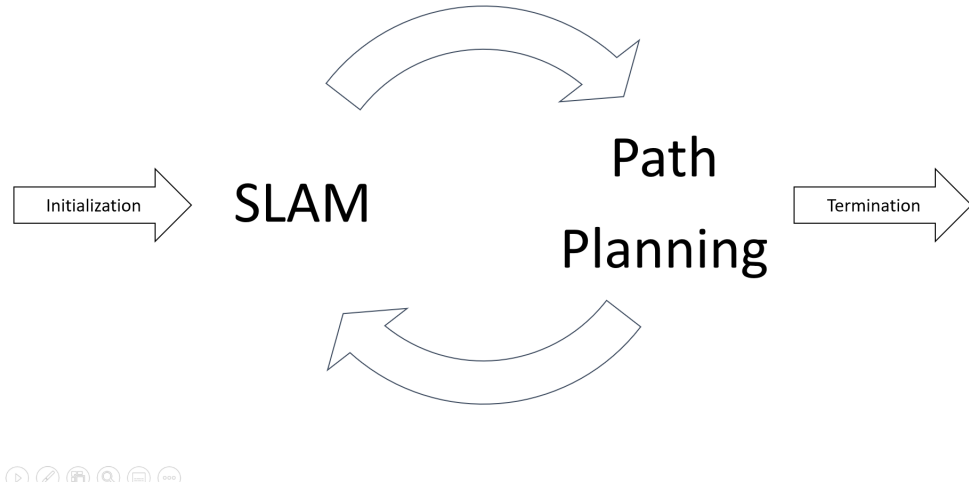


Figure 1: Automated exploration system, based on a SLAM algorithm and a path planning algorithm.

This work targets to answer two distinct research questions.

1. What is the most suitable open-source monocular visual SLAM algorithm for an exploration task?

This paper is limited to evaluate monocular visual SLAM (vSLAM) algorithms, meaning that the algorithm is only working with a single RGB (red, green, blue) camera as sensor. Therefore, since nowadays RGB cameras are either a standard on drones or can easily be upgraded, these drones are very affordable, making it highly available for a larger user group.

Thus, for this first part of this work, three open-source monocular visual SLAM algorithms are evaluated. DSO (Direct Sparse Odometry) SLAM, DSM (Direct Sparse Mapping) SLAM and ORB (Oriented FAST and Rotated BRIEF) SLAM were investigated regarding the predefined

criteria of the accuracy of the resulting trajectory estimation, the point cloud accuracy and computational speed.

This was done by using the publicly available benchmark EuRoC dataset [2], containing video sequences filmed by a drone, the ground truth of the position of the drone and the point cloud of the environment. Thus, the three SLAM algorithms are applied on the video sequences, the resulting trajectories and map points are compared to the ground truth regarding the above-mentioned criteria.

2. How can a framework be set up, where fully automated exploration systems can be tested and developed within a simulated environment?

In the second part of this work, a Roboter Operating System (ROS) framework, that enables users to develop a fully automated exploration system within a virtual environment is suggested. This framework includes a process, that provides a simulated Gazebo environment, making it possible to navigate a virtual drone within a simulated environment. The sensors and behavior of the drone are modeled realistically. Most importantly, the drone is equipped with a RGB camera, making it possible to directly apply a vSLAM algorithm on the output. Furthermore, the most suitable algorithm, evaluated in the first part of the work is implemented in a subprocess of this framework.

While the functionality and current state of the art of methods tackling the path planning task of the automated system are described and a suggestion on how it could be implemented into the framework are given in section 3.1.6, this work doesn't include an actual implementation of such an algorithm. Such implementations are left for further research.

The suggest framework should rather function as an option for users to implement and test out new path planning algorithm, providing optimal prerequisites to do so.

For example, the subprocess of the framework, in which the path plan-

ning algorithm should be running can be provided with all necessary data, such as sensor data of the drone and the estimated orientation, position and point cloud by the vSLAM algorithm. This stream data is preprocessed and standardized in real time, enabling users to directly use it for their purposes.

## 2. Evaluation of the vSLAM Algorithms

### 2.1 Related Work

#### 2.1.1 Introduction and History of SLAM

SLAM algorithms have to solve a chicken-egg-problem, since in order for the robot to localize itself within a unknown environment, it needs a map. However, for building a map, the robot needs to localize itself within it [1]. Until today, multiple different solutions for the problem were developed.

Today, the problem can be formally defined in a probabilistic way. The goal is to compute

$$\mathbb{P}(m_{t+1}, x_{t+1} | z_{1:t+1}, u_{1:t}), \quad (2.1)$$

where,  $m_{t+1}$  is the map (point cloud of the surroundings) at timepoint  $t + 1$ ,  $x_{t+1}$  the camera orientation and position at timepoint  $t + 1$ ,  $z_{1:t+1}$  all observations made to this timepoint and  $u_{1:t}$  all historic control input. In other words, a map and a series of positions should be computed, that fit the seen environment and the control inputs in the most likely manner. However, most modern SLAM methods do not require the control input anymore but rather predict the next position with a motion model and validate it with an optimization process.

[10] [21]. This problem overview is displayed in figure 2.

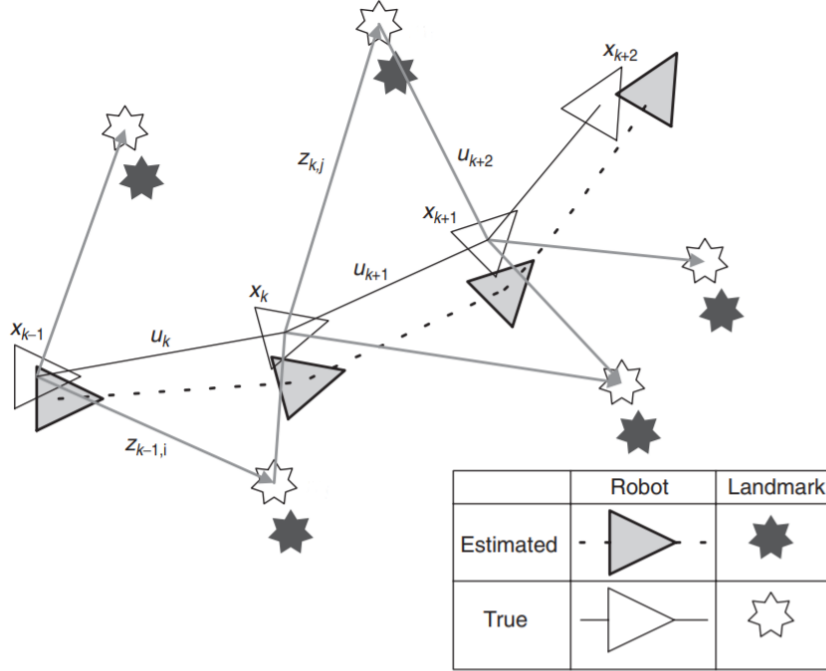


Figure 2: Overview of the SLAM concept. Source: [8]

With their work on the representation and estimation of spatial uncertainty [27] Smith et al created the first relevant work in the field on SLAM in 1986. However, due to lacking computational resources, the engagement in this topic stayed mainly on a theoretical level.

Work by Smith and Cheesman and Durrant-Whyte established a statistical basis for describing relationships between landmarks and manipulating geometric uncertainty. A key element of this work was to show that there must be a high degree of correlation between estimates of the location of different landmarks in a map [8].

Their work suggested for the first time, that the estimation should be based on a large vector, containing all landmark observations, as shown in the formal definition of the problem in expression .

The first recognizable developed SLAM algorithms relied on optimization methods based on an extended Kalman filter, which is a non-linear state estimation approach by relying on a joint distribution of all measurements [29]. The first monocular vSLAM algorithm, developed in 2003, is based on the extended Kalman filter and is called MonoSLAM [6].

The computational cost of the MonoSLAM algorithm, and most other vSLAM algorithms grows in proportion to the number of observed features, making it very hard to obtain real-time computation for medium or large environments [? ]. Obviously, an algorithm runs in real-time, when the algorithm can process the images, that are fed to it, just as fast as they are produced. Ideally, it should be running recognizably faster on average, since processing time per image can fluctuate.

In 2007, PTAM contributed with improvements by not running the tracking and mapping processes sequentially, like previous approaches, but rather to run these processes in parallel on two distinctive threads [14].

Then, more and more direct monocular visual vSLAM algorithm were developed. Unlike previous feature-based approaches, direct algorithms use the entire image as input in order to compute the term in expression 2.1.1. Therefore, the term is computed by optimizing the photometric error, which is the error, that results from comparing the intensities of each pixel after transformation [10].

One of the main benefits of a direct formulation is that it does not require a point to be recognizable by itself, thereby allowing for a more finely grained geometry representation (pixelwise inverse depth). [10]

Feature based methods on the other hand, compute features for each frame, that serve as input for further computation. These features usually are subsets

of pixels, that have remarkable intensities and arrangements, such as corners (landmarks). These methods evaluate the upper term by computing the geometric error, since the feature-positions are geometric quantities. A main advantage of feature based methods is the robustness over geometric distortions present in every-day-cameras [10].

While multiple evaluation studies exist [13] [24] [33] [21], [10], the comparison of the results is difficult.

One of the main benefits of a direct formulation is that it does not require a point to be recognizable by itself, thereby allowing for a more finely grained geometry representation (pixelwise inverse depth). [15]

On the one hand, the difficulty lies in the dependency of the results on the choice of the alignment method, that transforms the resulting output of the vSLAM algorithm to the reference frame of the ground truth. A different alignment function will result in a different result. This even led to a proposal of an evaluation method, that is not dependent on the ground truth reference frame [15]. However, the proposed method has to be computed by performing manual steps, and therefore never became the standard.

Also, the usage of different error metrics, the usage of different benchmark datasets and difference in computational power of the systems, on which the evaluation took place, can cause differences in results. Finally, the accuracy of the point cloud, which is a crucial part for our proposed framework in the second part of this work to function correctly, has rarely been studied [33].

Therefore, in this chapter, DSO-, DSM- and ORB SLAM are compared using the performance indicators explained in section 2.2.

Of all existing vSLAM algorithms, this evaluation considers DSO-, DSM- and ORB SLAM for the evaluation of being a suitable candidate for the autonomous

exploration task. ORB-SLAM was considered, because it showed the very good results in different evaluations [13] [20]. DSO-SLAM yield also good accuracy [20], and states to be able to track through scenes with very little texture, where feature based methods fail [10]. Finally, DSM states to be the most accurate direct SLAM method [37].

In the following section, an overview over how the algorithms work is given for each method. In order to understand this section, it is crucial to clarify basic definitions and vocabulary used in SLAM first.

### 2.1.2 Definitions

#### Keyframe

Most vSLAM Algorithms make usage of so called keyframes, as these keyframe-based approaches have proven to be more accurate [28]. Keyframes are specific selected images of the input sequences or video streams. In most cases, the keyframes store all of the existing map points and all of the computations and optimizations are made, based on the keyframes and data stored within them.

#### Covisibility Graph

Some algorithms create a covisibility graph in order to link keyframes and gain more information about the environment by having a different representation. In a covisibility graph, nodes are representing features and edges the covisibility between them. This can help the algorithms to perform optimizations and loop closing as explained in the following section. updating the edges resulting from the shared map points with other keyframes.

### Group of Rigid Transformations in 3D

$\text{SE}(3)$  is the group of rigid transformations in 3D space [9]. Each Matrix  $T \in \mathbb{R}^{4 \times 4}$  with

$$T = \begin{bmatrix} R & t \\ 0 & 1 \end{bmatrix}$$

and  $R \in \mathbb{R}^{3 \times 3}$  being a rotation matrix and  $t \in \mathbb{R}^3$  a translational vector, is an element of  $\text{SE}(3)$ .

Sometimes, instead of representing the orientation by the rotation matrix  $R$ , the orientation is given by so called quaternions  $q \in \mathbb{R}^4$ . The transformation between these two standards is possible.

### Point cloud

When we speak of point cloud, we simply mean a formation of points in the three-dimensional space, though having an x y and z coordinate. Later in the evaluation of the algorithms, to save these point clouds, the PLY format has been chosen.

### Camera Calibration and Distortion

For a SLAM algorithm to work with multiple camera types, such as fisheyes cameras, the camera input has to be standardized. Therefore, different parameters must be provided. These parameters include

- The image size
- The focal lengths (x and y)

- The optical centers (x and y)
- The distortion parameters

The calculations of the resulting transformation in order to gain a standardized image, can be found in the OpenCV documentation.

### 2.1.3 ORB-SLAM

ORB SLAM is a feature based, state of the art slam method. The first version was published in 2015 [21]. Here, an overview of the functionality of ORB SLAM is provided. The Algorithms runs on three threads simultaneously. Each thread performs one of the following tasks: Tracking, Local Mapping and Loop Closing. An overview over the tasks can be found in figure 3. The explanation of these system components are described in the following subsections. A more detailed explanation can be found in the paper of Raul Mur-Artal et al [21].

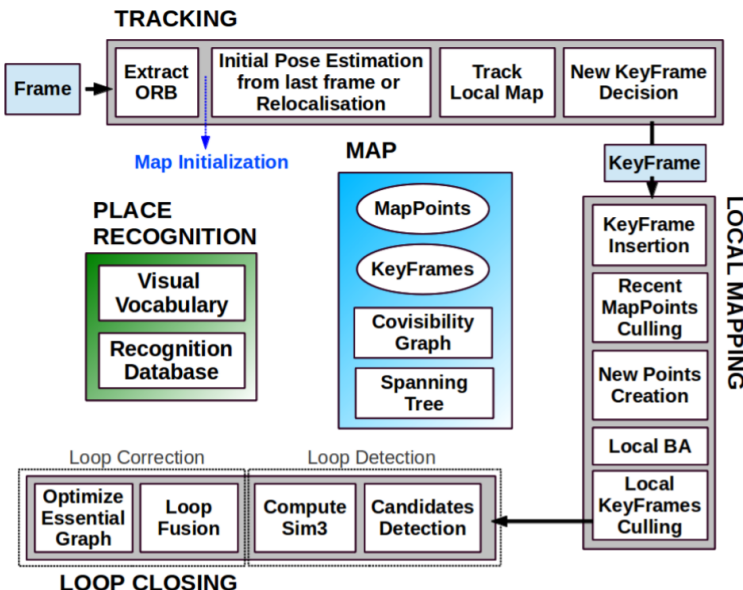


Figure 3: Overview of the system components extracted from [21]

## Tracking

The tracking component determines the localization of the camera and decides, when a new keyframe is being inserted. As it is shown in figure 3, the tracking is performed in four steps.

### 1. Feature Extracting

Features are extracted using Oriented FAST and Rotated BRIEF [25]. This method starts by searching for FAST (Features from Accelerated and Segments Test). Therefor, for each pixel  $x$  in the image, a circle of 16 pixels around that pixel are considered and checked if at least eight of these 16 pixels have major brightness differences. If so, the pixel  $x$  is considered as a keypoint, since it is likely to be an edge or corner. This is repeated multiple times after downsizing the image up to a scale of eight. To extract features evenly distributed over the image, it is divided into a grid, trying to extract five features per cell. Extracting features this way, makes the algorithm more stable to scale invariance. Next the orientation of the extracted feature is calculated using an intensity centroid. Finally the features are converted into a binary vectors (ORB descriptor) using a modified version, which is more robust to rotation, of BRIEF descriptors (Binary robust independent elementary feature). These ORB descriptors are then used for all feature matching tasks.

### 2. Initial Pose Estimation

A constant velocity model is first run to predict to the camera pose. Then, the features of the last frame are searched. If no matches are found, a wider area around the last position is searched.

### 3. Track Local Map

When the camera pose is estimated, map point correspondences are searched in the local map, containing keyframes that contain the ob-

served map points and the keyframes from the covisibility graph. The pose is then corrected with all matched map points.

#### 4. New Keyframe Decision

To insert the current frame as a keyframe, the following conditions have to be met: more than 20 frames have to be passed from the last relocalization or keyframe insertion (when not idle), the current frame tracks at least 50 points or less than 90 percent of the points of the keyframe in the local map with the most shard mappoints.

### Local Mapping

Whenever a new Keyframe  $K_i$  is inserted, the map is updated.

#### 1. Keyframe Insertion

The keyframe is inserted in the covisibility graph. Then the spanning tree is updated using the keyframe with the most common points with  $K_i$ . Finally the keyframe is represented as a bag of words using the DBoW2 implementation. Therefor, the image is saved by the number of occurrences of features found in a predefined vocabulary of features. When the vocabulary is created with images general enough, it can be used for most environments.

#### 2. Recent Map Points Culling

A map point is removed from the map, when it is found in more than 25/it must be observed from more than two keyframes if more than one keyframe has passed from map point creation.

#### 3. New Map Point Creation

A map point is created by calculating the triangulation of the connected keyframes in the covisibility graph. For each map point, the 3D coordinate

in the world coordinate system, its ORB descriptor, the viewing direction, the maximum and minimum distance at which the point can be observed is stored.

#### 4. Local Bundle Adjustment

The keyframe poses  $T_i \in \text{SE}(3)$  and Map Points  $X_j \in \mathbb{R}^3$  are optimized by minimizing the reprojection error to the matched keypoints  $x_{i,j} \in \mathbb{R}^2$ . The error is computed by the following term:

$$e_{i,j} = x_{i,j} - \pi_i(T_i, X_j)$$

.  $i$  is the respective Keyframe and  $j$  the index of the map Point.  $\pi_i$  is a projection function, calculation a transformation to project all keypoints on map points by minimizing a cost function, that can be found in [31].

In case of full BA (used in the map initialization) we optimize all points and keyframes, by the exception of the first keyframe which remain fixed as the origin. In local BA all points included in the local area are optimized, while a subset of keyframes is fixed. In pose optimization, or motion-only BA, all points are fixed and only the camera pose is optimized [21] .

At this point, a local BA is performed.

#### 5. Local Keyframe Culling

With difference to other SLAM algorithm, ORB slam deletes redundant keyframes, which decreases computational efforts, since computational complexity grows with the number of keyframes. All keyframes are deleted, where at least 90 percent of the map points can be found in at least three other keyframes.

## Loop Closing

The loop closing is computed based on the last inserted keyframe  $K_i$ .

### 1. Loop Candidates Detection

First the similarity of  $K_i$  to its neighbors in the covisibility graph is computed by using the bag of words representation and a loop candidate  $K_l$  might be chosen.

### 2. Similarity Transformation

In this step the transformation is computed, to map the map points from  $K_i$  on  $K_l$ . Since scale can drift, also the scale is computed in addition to the rotation matrix and translation using the method of horn.

### 3. Loop Fusion

Here, duplicated map points are fused and the keyframe pose  $T_\omega$  is corrected by the transformation calculated in the previous step. All map points of  $K_l$  are projected in  $K_i$ . All keyframes affected by the fusion will update the edges (shared map points) in the covisibility graph.

### 4. Essential Graph Optimization

Finally, the loop closing error is distributed over the essential graph.

## Complement

Please note, that this is the base model of ORB-SLAM. Multiple amendments, forks and merge requests exists, either made by the creators themselves, or by external developers. Though it was slightly abbreviated for our purposes, in the evaluation part of this work, ORB-SLAM3 is used.

The main feature that was added in this version and also affect the result, is the possibility to create multiple maps within one session. If the tracking is

lost, simply a new map is created. When places are then revisited, the maps get merged and the tracking can therefore resumed normally. This way, good performance results can be yielded, even with long periods of poor visual information [3].

In the second part of this work, ORB-SLAM2 was used. This is simply due to the fact, that compiling other versions on the platform described in the second chapter failed. However, for the monocular usage, to the authors best knowledge, no main differences are made to the above-described version.

### 2.1.4 DSO-SLAM

Direct Sparse Odometry was developed in 2016 by the Technische Universität München.

#### Model Overview

The model optimizes the photometric error over a window of recent frames.

The camera is calibrated in two different ways. First a projection function is computed, considering the focal length and the optical centers, in order to map a pixel point in the image on a 3D map point (and the other way around). Secondly, a photometric camera calibration is applied. This calibration accounts for camera specific non-linear response functions, that map scene irradiances on pixel intensities on the one hand and camera specific lens attenuation on the other hand.

The model relies on minimizing the photometric error. This error over all frames is given by

$$E_{\text{photo}} := \sum_{i \in \mathcal{F}} \sum_{p \in \mathcal{P}_i} \sum_{j \in \text{obs}(p)} E_{pj}, \quad (2.2)$$

where  $\mathcal{F}$  is the set of all frames,  $\mathcal{P}_i$  the set of all pixel in frame  $i$  and  $\text{obs}(p)$  the set of indices of frames, where the point  $p$  occurs.  $E_{pj}$  on the other hand is the difference in pixel intensities, calculated by the huber norm, after mapping the pixels on each other and applying an additional affine brightness transfer function. Also,  $E_{pj}$  does not only include comparing the point  $p$ , but also computes the pixel intensity difference of eight pixel neighbors of  $p$ , arranged in a spread pattern. This pattern is shown in figure 4.

Our experiments have shown that 8 pixels, arranged in a slightly spread pattern [...] give a good trade-off between computations required for evaluation, robustness to motion blur, and providing sufficient information

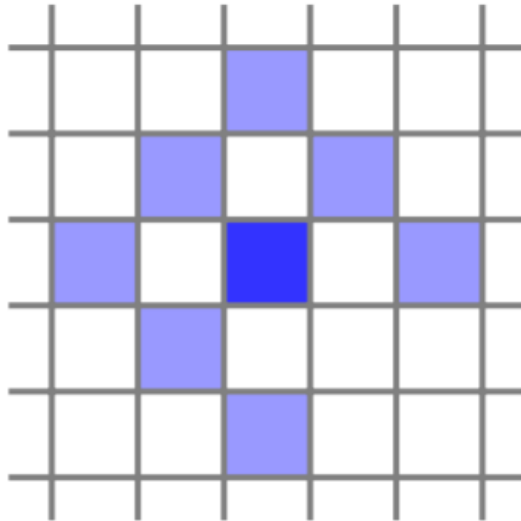


Figure 4: Neighbor pixels considered for the photometric error calculation.  
Source: [10]

## Visual Odometry Front-End

The front end determine the sets  $\mathcal{F}$ ,  $\mathcal{P}_i$  and  $\text{obs}(p)$ . Also it initializes all parameters required to calculate the term 2.1.4. Finally it decides, when to remove points, outliers and keyframes. Frame and point management are closer described in the following.

### 1. Frame Management

If a new keyframe is created, all map points are mapped into it. In case the root mean squared error of the current frame is more than twice as high than the one before, direct image alignment is assumed to have failed and initialization is tried again. The algorithm tries to always work with seven active keyframes. All computations are made in reference to those keyframes.

For creating a new keyframe, 5-10 frames per second are considered for creation. A keyframe must meet all of the following requirements:

- (a) The field of view changes.
- (b) Camera translation causes occlusions.
- (c) Camera exposure time changes significantly.

When deciding when to marginalize a keyframe, following roles are applied to the active keyframes  $I_1, \dots, I_7$ , with  $I_1$  being the most recent:

- (a)  $I_1$  and  $I_2$  are always kept.
- (b) keyframes, whose number of points contained in  $I_1$  is less then 5 percent are marginalized.
- (c) If still too many keyframes are active, the ones having the largest distance to  $I_1$ , or the worst distributed in 3D space are removed.

## 2. Point Management

DSO always tries to keep 2000 active points in the map. The first step is select candidates points of the frame. To obtain equally distributed points, the image is split into blocks. In each block, the point with the largest gradient of pixel intensity is selected, if it is greater than a threshold, which is computed by adding seven to the overall median of the gradients. This is repeated twice while decreasing the threshold and doubling the block size, in order to also include points with weaker gradient. By gradient, simply the change of pixel intensities to all neighbors is meant.

Then, the point candidates are tracked in subsequent frames by minimizing  $E_{pj}$ . From the best match, the depth value is initialized.

When old points are marginalized, candidate points are activated in a way that points in the active map are as evenly distributed as possible. This is achieved by always selecting the point, which offers the largest distance to the next active point, after projecting it into the last active keyframe.

Since outlier only consume unnecessary resources, they are tried to be removed. For example, point for which  $E_{pj}$  surpasses a threshold are removed permanently.

### 2.1.5 DSM-SLAM

Direct Sparse Mapping SLAM was released in april 2019 and works similar to DSO slam but claims to be more robust when revisiting areas. The algorithm can be separated into a tracking front-end and an optimization back-end that run on parallel threads.

## Model Overview

DSM uses the same model as DSO. The model is described in the previous section.

## Front-End

The front-end, however, differs from DSO. While DSO cannot reuse points that have once been marginalized, DSM suggests a method to activate and deactivate keyframes and points to its needs.

### 1. Keyframe and map point selection

When selecting keyframes and map points, two criteria play a role: the temporal and covisibility criteria. The temporal part regards  $N_t$  keyframes as recent sliding window approach, just like DSO. With similar criterias for keyframe selection as DSO, whenever a new keyframe is inserted, another one is removed (from the temporal part).

In order to regard re-observed points, DSM also considers  $N_c$  covisible keyframes to fill the latest keyframe  $I_0$  with map points, favoring map points in depleted areas. This is achieved by the following steps:

#### (a) Identify depleted areas

All map points from the temporal part are mapped into the latest keyframe. For every pixel, the euclidean distance to the closest map point is computed. Obviously, large distances suggest depleted areas.

#### (b) Covisibil keyframe selection

Select the keyframe within the old keyframes with the most map points in the above selected depleted area. Map points, where the viewing angle lies too far from the latest keyframe are removed from

the local map. This can be determined from the pose  $T_i \in \text{SE}(3)$  that is saved for each keyframe  $I_i$ .

(c) Update distance map

Update the distance map, calculated in step 2, with the new selected keyframe.

(d) iterate

Iterate until  $N_c$  keyframes are selected for the covisibility part.

The entire keyframe and map point selection is displayed in figure 5. In this case,  $N_t$  is equal to four and  $N_c$  is equal to three.

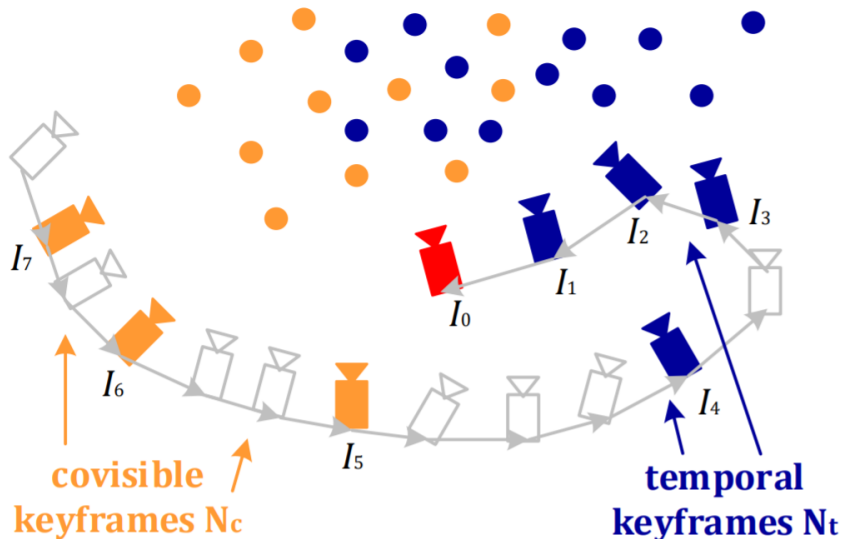


Figure 5: Keyframe and Point Selection of DSM. Source: [37]

## 2. Frame Tracking, New Keyframe decision, New Map Point Tracking

Frame Tracking, New Keyframe decision and New Map Point Tracking work similar to DSO SLAM. The main idea is always to manipulate the local map by minimizing the photometric error displayed in equation ??.

However, unlike DSO SLAM, in each frame, the local map consisting of the  $N_t + N_c$  keyframes (referenced from the latest keyframe) and contained map points is projected into the frame. Obviously, this also brings the

difference compared to DSO slam, that keyframes and map points are not permanently culled from the map, and may be reactivated once the keyframe appears in the covisibility graph. Also, the management of outliers is similar to DSO-SLAM, Trying to remove outliers as early as possible, in order to save computational resources.

## 2.2 Evaluation Methods

To evaluate the performance of DSO-, DSM- and ORB-SLAM, the algorithms are fed with video sequences contained in the European Robotics Challenge (EuRoC) benchmark dataset. The algorithms are changed in a way, that they save the computed trajectory estimation to a .txt file and the resulting point cloud to a .PLY file.

Because an algorithm run on the same sequence can yield different results, each sequence is fed three times to the algorithm. This way, the results are more reproducible.

### 2.2.1 Dataset

For the evaluation of the vSLAM Algorithms, the EuRoC dataset [2] was used. The dataset contains eleven video sequences, recorded with a micro aerial vehicle at 20 frames per second. The sequences have an image resolution of 752x480 pixels.

For each Sequence, RGB images from two cameras exist. However, since the evaluation focuses on monocular SLAM methods, only the left camera was considered. Also the available inertial and camera pose data was not taken in consideration.

The first five sequences were recorded in the machine hall of the Eidgenössische Technische Hochschule Zürich, and the other six were recorded in a room, that was provided with additional obstacle. For the latter six sequences, the ground truth of the environment exists as a dense point cloud, as can be seen in figure 6.

Finally the true camera pose  $\in \text{SE}(3)$  of the camera is known at a high frequency

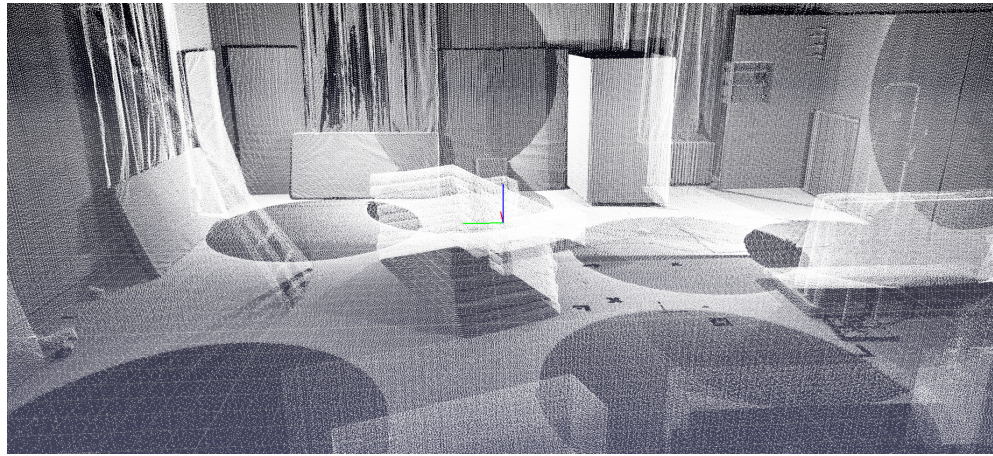


Figure 6: Point cloud ground truth of sequence V1\_01\_easy visualized with python package pptk

of over 200 points per second. This includes the camera position and the camera orientation.

An overview of the sequences is shown in table 1. For each sequence, the average camera velocity, rotation velocity duration are given.

### 2.2.2 Evaluation Criteria

#### Trajectory Comparison

##### 1. Trajectory Alignment

In order to compare the evaluated position of the camera at a given time with the ground truth of the position, the trajectories need to be aligned. This is because most SLAM Algorithms initialize the origin of their coordinate system with the camera position from the first frame. Whereas the ground truth of the trajectory uses a different origin and orientation. As a consequence, evaluated points  $\{\hat{x}_i\}_{i=0}^{N-1}$  can not be compared to the ground truth points  $\{x_i\}_{i=0}^{N-1}$ . Also, as described in the vSLAM Algorithms section, the minority of the existing vSLAM algorithms are recognizing the true

Table 1: Overview of the sequences included in the EuRoC Dataset

Sequence Name	Duration in s	Average Velocity in $ms^{-1}$	Point cloud available
MH_01_easy	182	0.44	No
MH_02_easy	150	0.49	No
MH_03_medium	132	0.99	No
MH_04_difficult	99	0.93	No
MH_05_difficult	111	0.88	No
V1_01_easy	144	0.41	Yes
V1_02_medium	83.5	0.91	Yes
V1_03_difficult	105	0.75	Yes
V2_01_easy	112	0.33	Yes
V2_02_medium	115	0.72	Yes
V2_03_difficult	115	0.75	Yes

scale of the coordinate system. For those two reasons, the target is to find  $S = \{R, t, s\}$ , while  $R$  being a rotation matrix,  $t$  a translation vector and  $s$  a scaling factor, such that

$$S = \arg \min_{S'=\{R', t', s'\}} \sum_{i=0}^{N-1} \|x_i - s'R'\hat{x}_i - t'\|^2$$

In other words, the evaluated points are rotated, translated and scaled in a way, that the sum squared error over the respective point distances is minimized. The upper expression is calculated by using the method of Umeyama [32].

Similar to principal component analysis, Umeyama uses the singular value decomposition of the covariance matrix  $\Sigma$  of  $x$  and  $\hat{x}$ . Thus,  $\Sigma = UDV^T$  is yielded. Umeyama proves, that  $R, t$  and  $s$  can be calculated as followed:

$$R = UWV^T$$

$$s = \frac{1}{\sigma_p^2} \text{tr}(DW)$$

$$t = \mu_{\hat{x}} - sR\mu_p$$

with

$$W = \begin{cases} I, & \text{if } \det(U) \det(V) = 0 \\ \text{diag}(1, 1, -1), & \text{otherwise} \end{cases}$$

$\sigma_p$  being the standard deviation of  $x$ ,  $\mu$  the mean and  $\text{tr}$  the trace of a matrix.

## 2. Positional Error

The error between  $\{\hat{x}_i\}_{i=0}^{N-1}$  and  $\{x_i\}_{i=0}^{N-1}$  is computed after aligning them with the upper method using the computed parameters  $S = \{R, t, s\}$ , yielding

$$\hat{x}'_i = sR\hat{x}_i - t$$

. Then the distances between the points are evaluated using the euclidean norm:

$$e_i = \|\hat{x}'_i - x_i\|_2$$

In figure 7 the computed errors are displayed.

These error terms are visualized over time and the overall mean is determined and again visualized with boxplots for each method. Additionally, the flight paths are plotted against each other after alignment, to gain visual information of the trajectories. This is done for all three axes.

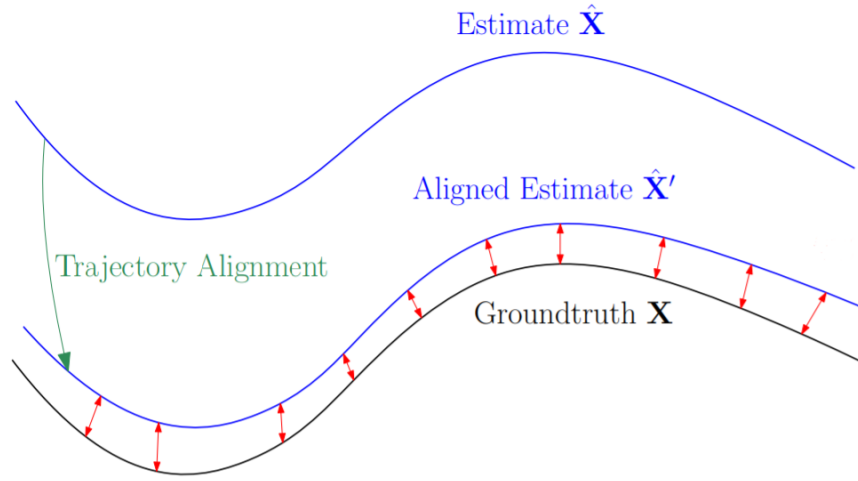


Figure 7: Trajectory error after alignment. Source: [36]

### Point cloud evaluation

The algorithms were manipulated in a way, that after evaluating each sequence, they write a .PLY file with all map points to the device. These map points are then evaluated by the following methods. Obviously, this is only done for latter six sequences, where a ground truth of the point cloud exists.

Additionally to the following methods, the point clouds are visually observed, trying to figure out, if the SLAM algorithms are also able to detect small obstacles, which is crucial for a successful autonomous navigation of the drone.

#### 1. Positional Error

Again, the map points are transformed using the method of umeyama. However, it is crucial to note that the computed  $S = \{R, t, s\}$  is not a result of aligning the point clouds, but rather the parameters for aligning the trajectories are used. This is done, to ensure, that trajectory and point cloud are transformed in the same way, and fit in the same world reference.

To compare the the transformed computed point cloud  $P' = \{\widehat{p'}_i\}_{i=0}^{M_{\text{eval}}-1}$  to the ground truth point cloud  $\{p_i\}_{i=0}^{M_{\text{gt}}-1}$ , for a point in the evaluated point

cloud, the distance to the closest point in the ground truth point cloud is calculated. This is assumed to be the points ground truth position, since with several 100000-points in ground truth, this point in the ground truth point cloud should not be too far away from the orthogonal projection of the evaluated point.

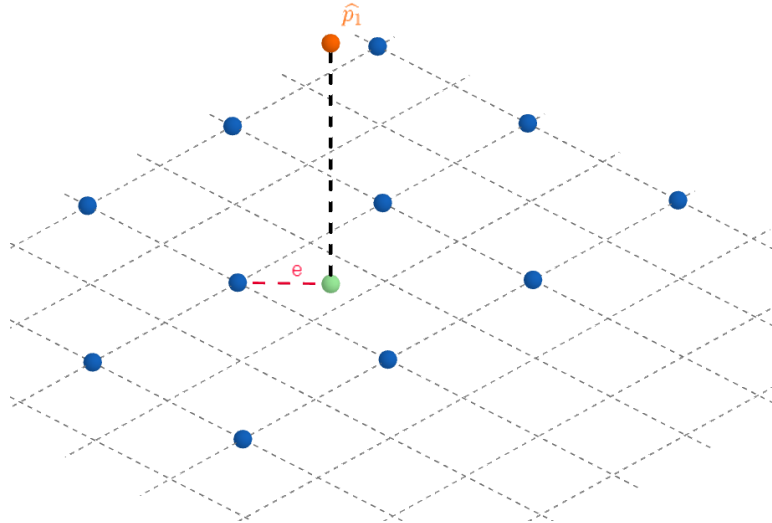


Figure 8: Orthogonal projection of a point in the evaluated point cloud ( $\hat{p}_1$ ) on the planar of the ground truth point cloud. The error  $e$ , determines how far the considered point for the ground truth lies from the actual point of the ground truth.

This situation is displayed in figure 8, where it gets clear, that the more points are available in the ground truth point cloud, the smaller is the distance in between them and therefore the smaller the error  $e$  becomes.

Since calculating distances from several 100000 points to several 100000 points is computational very expensive, and in the current setup applying it an all sequences and algorithms would require more than a day, only a subset of  $P'$  of 1000 points per sequence and algorithms is taken into consideration. The indices for the subset  $I_{\text{sub}}$  are sampled from a even distribution of  $i_{i=0}^{M_{\text{eval}}-1}$ . Then, as mentioned, distances to the closest point in the ground truth point cloud is calculated for the sampled subset  $P'_{\text{sub}} = \{\hat{p}'_i\}_{i \in I_{\text{sub}}} \subset P'$ .

The error term for  $\hat{p}_i' \in P'_{\text{sub}}$  is then given by

$$e_i = \arg \min_{j \in I_{i=0}^{M_{gt}-1}} \|\hat{p}_i' - p_j\|_2$$

These error terms are then plotted within a boxplot for each method over all sequences.

## 2. Density

As described in the second chapters, as a result of the functionality behind feature based methods, their evaluated point clouds are significantly less dense. To quantify the density, for each algorithm and sequence the absolute number of points generated by the algorithm is accessed.

## Computation Time

Since the computational performance of an algorithm is crucial to perform in real time, the absolute time that is needed to process each sequence is measured for each algorithm. The time required for initialization is subtracted, since it is not decisive for the assessment, if the algorithm can be run in real time. For each sequence the resulting speed is additionally evaluated in computed frames per second.

### 2.2.3 Setup and Environment

The entire evaluation is run on a virtual machine. The virtual machine is running through the program VirtualBox provided by oracle. The host system is a lenovo yoga with eight GB of RAM and the basic model (8250U CPU @1.6 GHz 1.80GHz) of an eight core i5. The operating system of the host machine is Windows 10 Home. The virtual machine is given 5 GB of Ram and 4 cores for

the computations. The operating system of the virtual machine is Ubuntu 18.04. All further setup information can be extracted from the github repository.

## 2.3 Results

The three SLAM algorithms were evaluated regarding the computed trajectories, the resulting pointclouds and the computational complexity.

### 2.3.1 Trajectory Evaluation

In order to evaluate the quality of the trajectory computed by the algorithms, the trajectory firstly had to be transformed into the world reference of the ground truth data. This is because the algorithms usually initialize the origin with the first (key)frame and the groundtruth data doesn't. Furthermore, monocular visual slam algorithms are generally not capable to extract the true scale. The alignment was performed using the method of Umeyama, described in the ?? section. After alignment, as a first indicator for the accuracy of the computed trajectories, the trajectories were visually observed by plotting the true position and the evaluated position into a coordinate system. The x, y and z axis were observed separately. This method for comparing the trajectories is described in detail in section ???. Obviously, trajectories, that align perfectly with the groundtruth suggest that the position was correctly evaluated by the algorithm.

In figure 9 the computed trajectories are plotted against the groundtruth for sequences MH01, V102 and V203 considering only the x and y coordinate. These sequences were selected, because they represent the results of the visual analysis well. In the first sequence, MH01, all algorithms showed excellent results. One reason for this could be, that in the first sequence, the camera only does very gentle movements, moving at an average speed of  $0.41ms^{-1}$ .

The second image shows the sequence V102. Here, ORB and DSM show good results, since in most parts, the trajectories are aligned perfectly. DSO on the

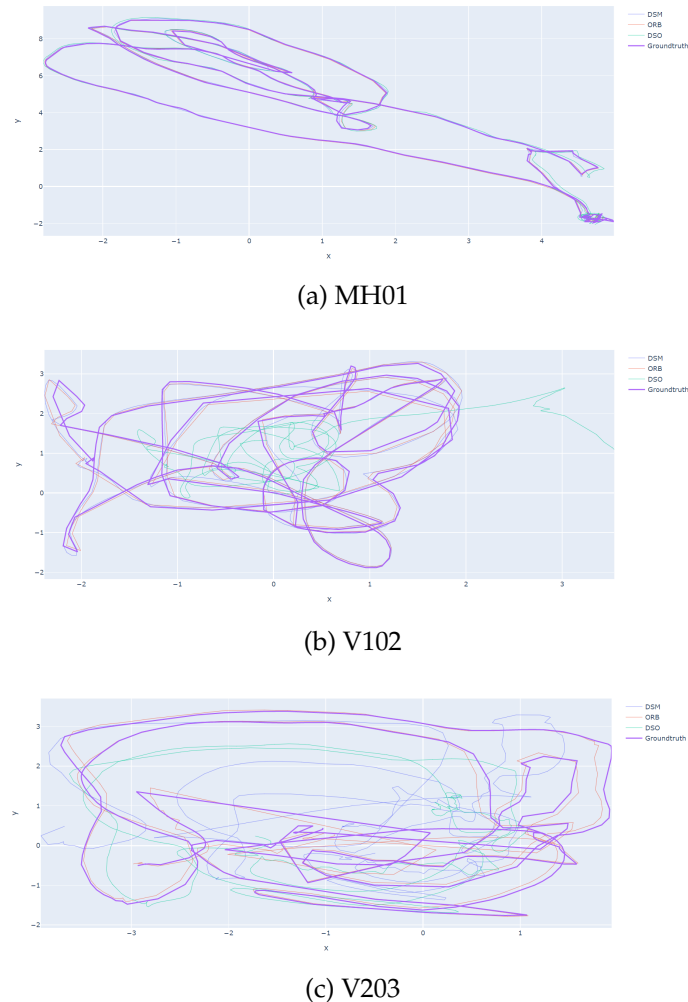


Figure 9: Ground truth flight path and evaluated flight path of each algorithm after alignment with the method of Umeyama in the x and y axis in meters. Left the sequence MH01, middle the sequence V102 and right the sequence V203 is displayed.

other hand shows a significant difference in the flight path. When observing the trajectory closely, the assumption is raised, that the algorithm lost tracking and therefore computed significant wrong position data. This might have caused the calculated positions in the right of the plot, that have a large distance to the groundtruth. The rest of the sequence might have been correctly estimated, however since the alignment is done minimizing ??, one significant mistake in the position estimation, might result in horrific results over the entire sequence after alignment. This is supported by watching the algorithm running and by the fact that in the plot, the trajectory looks very similar to the groundtruth, only with a significantly smaller scale.

The last plot shows the results of the last sequence. Here, all algorithms had problems estimating a position that comes close to the groundtruth position. ORB SLAM still showed acceptable performance.

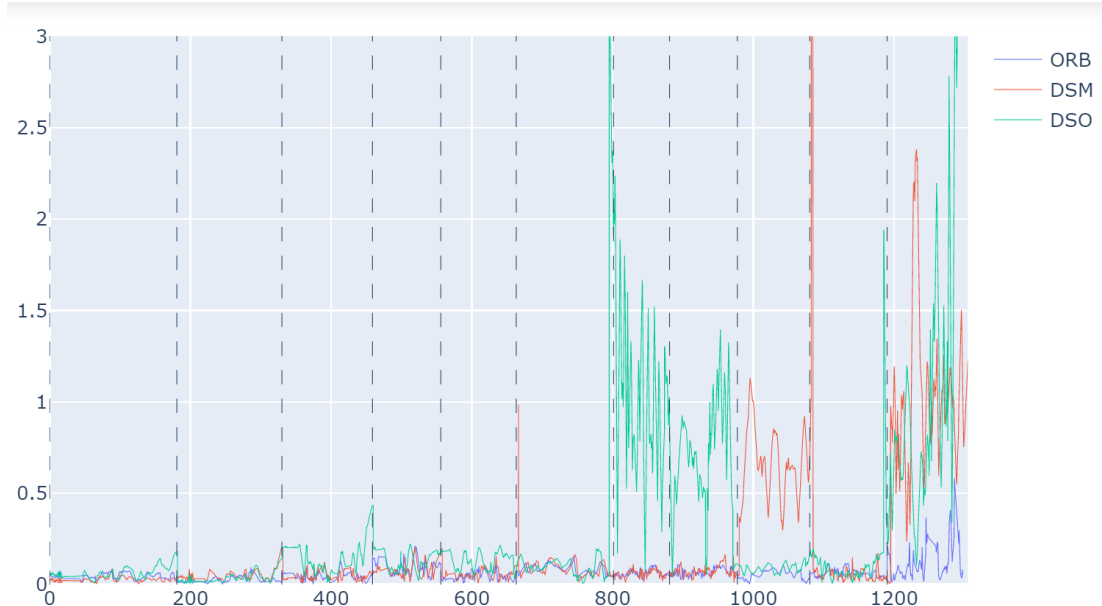


Figure 10: The positional error over time in meters. The vertical lines indicate the beginning of a new sequence

Furthermore, the Euclidean distances between position of the keyframe and the true position of the latter are computed. For a keyframe, the entry of the groundtruth data with the lowest distance in time to the time the keyframe was

inserted is taken as reference point. This is justifiable, since the true position is sampled at a frequency of over 200 points per second.

Figure 10 shows these distances over time for all sequences and for all algorithms. As suspected, in the first five sequences in the machine hall all algorithm performed good. The availability of more features in the scenery and the slow motions of the camera might explain the yielding of these results. Also, it can be noticed, that DSO SLAM drifts further apart from the ground truth position with the continuety of the sequence in the sequences MH01, MH03 and V202. This might be the result of lacking the functionality to close loops and to optimize over the global map, as explained in section ??.

In figure 11 a boxplot of all computed distances over all sequences is displayed. This plot summarieses the results of the trajectory analysis. The ORB algorithm, yielding a median positional error of 5.4 cm, performs slightly better than the DSO algorithm. DSO SLAM shows inconsistent results with a median positional error of more than 10cm and a large amount of errors greater than half a meter.

### 2.3.2 Pointcloud Evaluation

For the evaluation of the computed point clouds, these point clouds were first visually observed, as described in section ???. Figure 12 shows the evaluated point clouds aligned with the ground truth point cloud for sequence V101. This is a sequence, where the tracking of the trajectory was successfull for all three algorithms, thus, the errors of the resulting point clouds can not be a result of errors in alignment.

What becomes clear at first glance is, that as mentioned, ORB generates only few points, since only found keypoints are mapped in feature based methods. To give these points better visibilty, the point size was doubled in the ORB

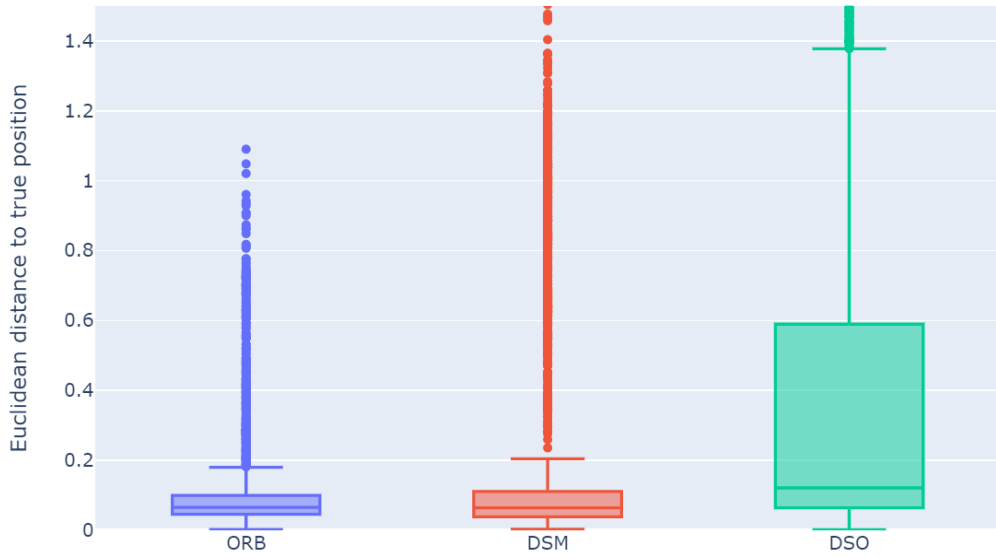


Figure 11: Boxplot of all euclidean distances between the ground truth position of the keyframe and the evaluated position after alignment with the method of Umeyama. Outliers greater than 1.5 are not displayed for clarity reasons.

image. DSM and DSO slam generate point clouds with significant higher density, where all structures of the room are clearly visible at first glance.

However, the advantage of ORB-SLAM over the other two direct methods is the recognizing of clear features in terms of structural differences in the scenes. Though, DSO and DSM also regard the differences in pixel intensities ORB, as described in section ??, detects the features on different scale levels and ensures, that the regarded features are in fact significant. This also became clear when observing the point cloud. All significant features, and therefore important features for autonomous navigation, were successfully marked with a computed point. For example, this can be seen at the leiter?? in image three of figure 12, where all sprossen contain at least one point.

After closely observing the point clouds, it became clear, that the point clouds of DSO, often times generate point clouds, where multiple layers of points were falsely generated, where all points had the same clear distance to the ground truth point cloud. This may be a result of working of DSO slam, where

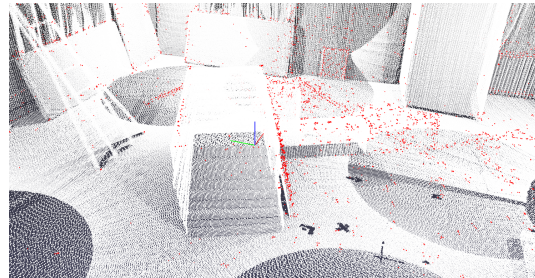
Table 2: Absolute number of points and distance to closest point in the ground truth point cloud in meter for each algorithm and sequence.

Sequence Name	ORB	DSM	DSO
MH_01_easy	8958 (/)	675720 (/)	361633 (/)
MH_02_easy	8692 (/)	700920 (/)	343804 (/)
MH_03_medium	7445 (/)	614264 (/)	371752 (/)
MH_04_difficult	7943 (/)	495752 (/)	208445 (/)
MH_05_difficult	8373 (/)	517712 (/)	232415 (/)
V1_01_easy	7075 (0.049)	6108440 (0.066)	374257 (0.066)
V1_02_medium	6517 (0.042)	648440 (0.187)	366513 (1.458)
V1_03_difficult	7983 (0.052)	775080 (0.092)	448212 (0.459)
V2_01_easy	5688 (0.049)	584552 (0.58)	247905 (0.086)
V2_02_medium	8129 (0.074)	733992 (0.078)	490608 (0.104)
V2_03_difficult	7359 (0.17)	921312 (0.645)	465396 (0.677)

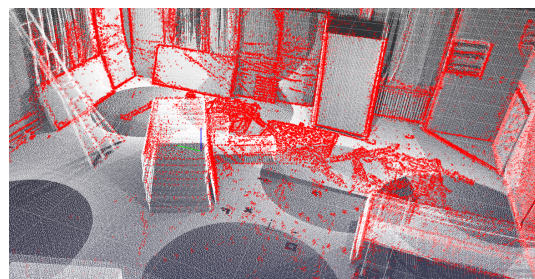
keyframes, that are marginalized, are removed permanently. When revisiting areas, the points are again generated. This means that all errors made in the sequence accumulate and when an area is revisited, significant errors in the point cloud can be made. This can be seen when looking at the third image closely. When looking at the matraccess in the middle of the room, the accumulated error expresses itself by points hovering in the air in a clear plane.

The density can also be expressed by numbers. The significant difference of the numbers of points can be seen in table 2. While ORB slam only generates close to 10000 points in the sequences DSM slam generates more than 500000 points in most sequences and DSO more than 200000 in most sequences.

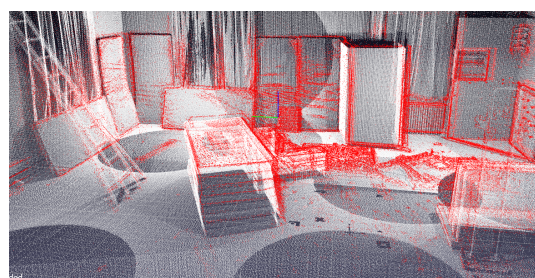
However, regarding the accuracy of the computed points by the algorithms, again ORB-SLAM shows the best performance. In table 2, for all sequences, where a groundtruth pointcloud exists, the distance to the closest point in the groundtruth point cloud is computed by randomly sampling 500 points



(a) ORB



(b) DSM



(c) DSO

Figure 12: The ground truth of the point cloud from Sequence V101 (white points) and the evaluated points by each algorithm (red points). The points in Figure (a) are twice as large for better visibility (ORB-SLAM generates only few points).

per algorithm and sequence. In all except the last, ORB-SLAM yields a mean distance of less than 10cm while DSM and DSO SLAM also yield results greater than 50 cm for certain sequences.

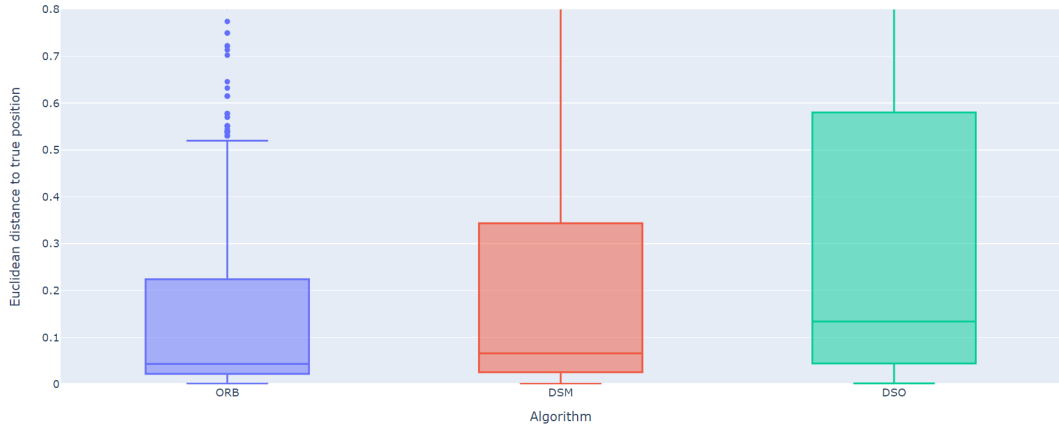


Figure 13: Boxplot of the euclidean distances between an evaluated point and the closest point of the ground truth point cloud. For computational feasibility, for each sequence and algorithm, 500 points for evaluation are sampled randomly

### 2.3.3 Calculation Time

For each sequence and algorithms, the computational time was taken, that the algorithm took, to complete the computation of the sequence. The time needed for initialization was not considered for the absolut time.

In order to evaluate, if an algorithm can run in realtime, the absolut times have to be broken down into the computed frames per second. The euroc dataset consists of sequences recorded at a frame frequency of 20 frames per second. This means the total frames per sequence are amount to  $\text{duration\_of\_sequence} \times 20$ . For the computed frames per second, this value is then devided by the time the algorithm needed to process the sequence.

It is possible to decrease the frame frequency, but this will also increase the risk

Table 3: Computation time (excluded time needed for initialization) of each sequence and algorithm. In parentheses the resulting computed frames per second are given.

Sequence Name	Computation Time in s ORB	Computation Time in s DSM	Computation Time in s DSO
MH_01_easy	257 (14,2)	1098 (3,3)	749 (4,9)
MH_02_easy	209 (14,4)	984 (3,1)	690 (4,4)
MH_03_medium	198 (13,3)	1369 (1,9)	707 (3,7)
MH_04_difficult	165 (12)	896 (2,2)	504 (3,9)
MH_05_difficult	193 (11,5)	825 (2,7)	633 (3,5)
V1_01_easy	253 (11,4)	1383 (2,1)	905 (3,2)
V1_02_medium	150 (11,1)	1550 (1,1)	820 (2,0)
V1_03_difficult	186 (11,3)	2262 (0,9)	1134 (1,9)
V2_01_easy	187 (12)	1045 (2,1)	612 (3,7)
V2_02_medium	162 (14,2)	1675 (1,4)	1522 (1,5)
V2_03_difficult	143 (16,1)	1600 (1,4)	793 (2,9)

of loosing the tracking, since the steps between the frames are greater and the ??forward motion model?? cannot predict the new position as well für einen gewissen algo.

The results are displayed in table 3. ORB-SLAM processes the frames at a frame per second rate ranging from 11,1 (V102) to 16,1 (V203), DSM SLAM processes the frames at a range from 0,9 (V103) to 3,3 (MH01) frames per second and DSO slam at a rate in range of 1,5 (V202) to 4,9 (MH01). Thus, none of the evaluated slam algorithms processes any of the evaluated sequences in realtime.

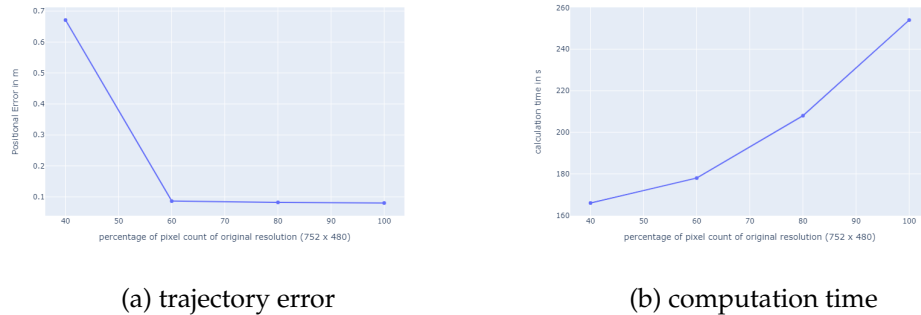


Figure 14: Influence of downsizing of the images on the trajectory error (a) and the computation time (b) for the sequence V101.

## 2.4 Discussion

### 2.4.1 Conclusion of SLAM-Algorithm Evaluation

### **3. Fully Automated Exploration System**

#### **3.1 Suggested ROS Framework**

In this section a framework to test and build an entire automated system is suggested. This framework includes a simulated environment, that realistically makes it possible, to navigate a drone within an simulated environment. The environment is based on the Roboter Operating System (ROS).

Just like our proposed system, most other automated exploration systems are based on the combination of a SLAM algorithm and a path planning algorithm [26] [23] [35] [22]. One example, where automated exploration with a drone is applied in real life is described in the work with the title A Fully-Autonomous Aerial Robot for Search and Rescue Applications in Indoor Environments using Learning-Based Techniques by Sampedro c. at al [26]. They propose a complex framework targeted for search and rescue operations. One issue, that becomes clear and will not be treated in our work, is the weight of the hardware, that is necessary to perform all computations onboard. While the drone in Sampedro's work had to compute even more processes, such as running a constitutional neural network for object classification, amounted to a total weight of 3.2 kg. Even if the drones for our purpose will not be as heavy, processing the computations onboard of an ardrone 2.0, as it is used in our simulation, is impossible. When taking our proposed framework to a real life scenario, as it is also discussed in this chapter, the drone would have to hold a wireless

connection (WIFI in case of the ARdrone 2.0) to a server, that does all the computations. Or, another drone would have to be used, in order to carry the hardware, that is needed for computation.

The basic idea of our framework can be seen in figure 1. The main parts of the automated exploration system are the SLAM Algorithm itself and the flight path planning algorithm, that work simultaneously. The general concept is that each of the algorithms takes the output of the other as input.

In the following section the suggested ROS framework is proposed and described in detail.

ROS stands for Roboter Operating System and as the name suggests, is a framework made to manage the software infrastructure within a robot. With the right drivers installed, it can access and use the robots hardware and serves as a messenger system between robot components. ROS packages make it easy to reuse important functionalities.

Gazebo on the other hand is an open-source 3D dynamic simulator for robotics. It can accurately and efficiently simulate robots regarding their physics and behavior. While gazebo simulations of drones can be created from scratch, this work relies on a framework, that was introduced by the robotics department of the Technische Universität München (TUM). Details can be found in section 3.1.1.

The suggested ROS setup consists of different nodes. Each node runs a process where certain computations are performed. These computations are based on input data and in most cases, the nodes also create data to output to the system. Within ROS, data is shared and received over so called rostopics (in short topics), which is a simple publish-subscribe-pattern for network communication. Each node can therefore publish the computed data over a certain topic or it can receive data from a certain topic by subscribing it. The frequency, the data is streamed to the system is also defined for each topic. The frequency the data

is received can also be manually defined for each subscription.

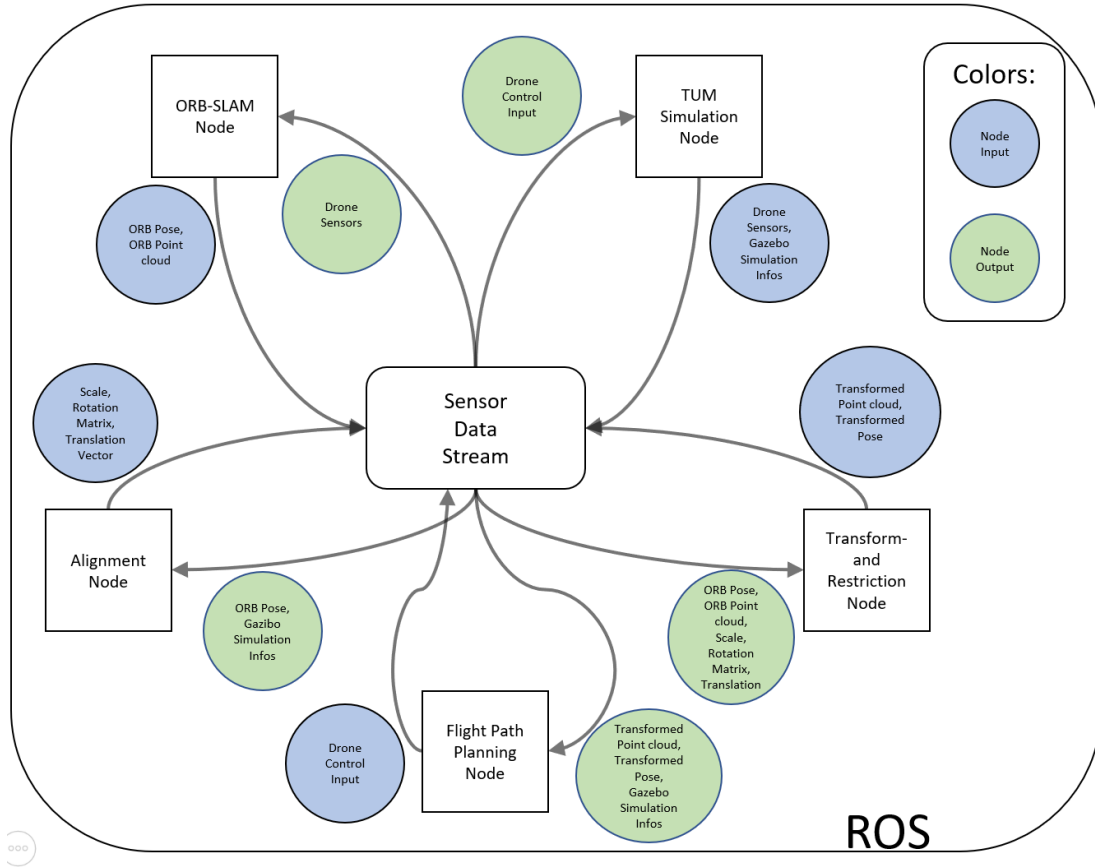


Figure 15: Overview over the suggested ROS framework for the simulated case

In figure 15 the suggested setup for an automated exploration framework within a virtual environment is displayed. The system consists of five nodes. While the functionality of the ORB-SLAM node, the TUM simulation node and the flight path planning node may be derived by previous section, such as the upper part of this section and the introduction, the functionality of the other two nodes have not been introduced.

To take advantage out of the fact, that running these algorithms in a simulated environment provides the system with information about the exact position of the drone and the position of simulated environment, these information must be processed. This is done in the alignment node and the transformation and restriction node.

The alignment node computes the parameters, that are needed to transform the reference frame of the ORB-SLAM algorithm to the reference frame of the gazebo simulation. The actual transformation of the point cloud and the pose computed by ORB-SLAM are then performed in the transformation and restriction node. Additionally, this nodes restricts the searching space of the path planning algorithm to a finite area. With the help of these two nodes, the system is then able to:

- Identify the true scale of the point cloud
- Confirm the correctness of the computed point cloud
- Confirm the correctness of the computed trajectory
- Limit the searching space of the path planning algorithm
- Feed the path planning algorithm with collision information of the drone
- Identify undiscovered spaces

Obviously, when testing the system in a real life environment, the ground truth of the position of the environment and drone are not available. Nevertheless, in order to get the true scale of the resulting point cloud, a modified framework is introduced additionally. This framework suggests an initialization process, that allows for an estimation of the position of the drone.

The functionality of all nodes are described in detail in the next sections.

Since the nodes are only dependent on each other in a way that they communicate over standardized messenges, they are independent of the programming language. This means that while the ORB-SLAM node is implemented in C++, all nodes developed explicitly for this framework are implemented in python with rosipy.

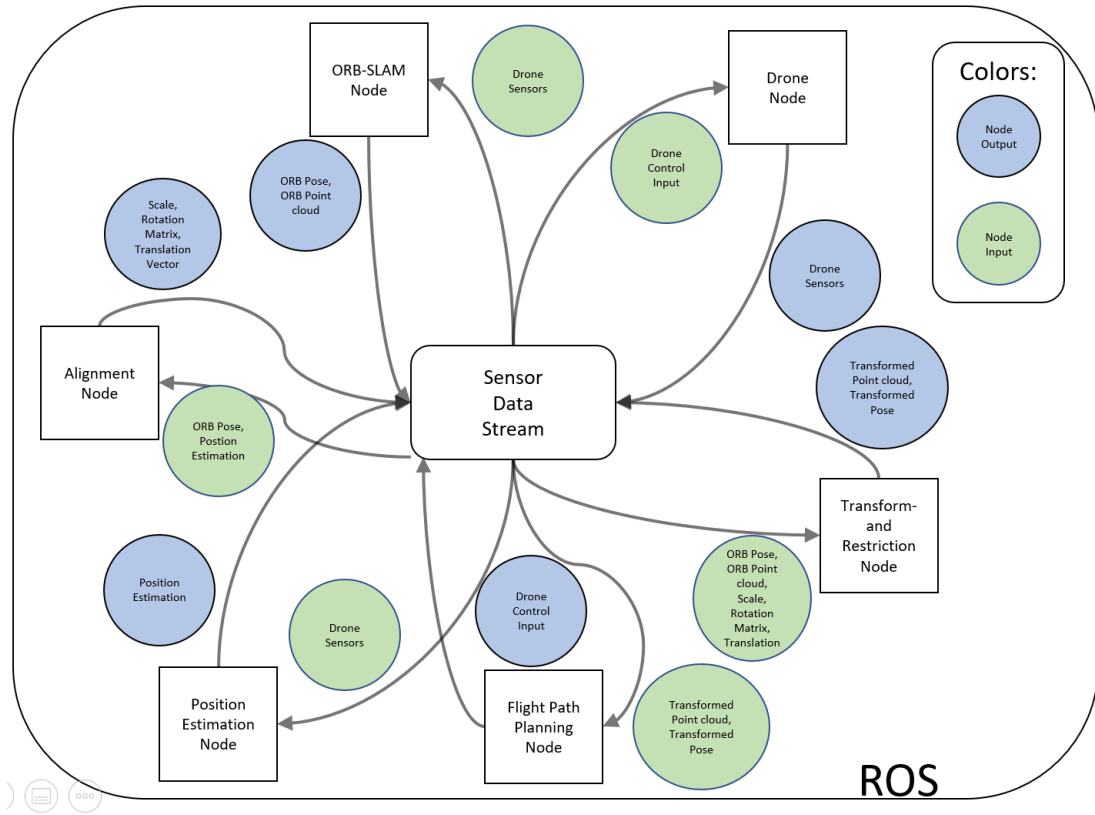


Figure 16: Overview over the suggested ROS framework for the real life case

### 3.1.1 TUM Simulation Node

Thus, with the `tum_simulation` package you can navigate an AR.drone 1.0 and 2.0 in different worlds created within gazebo. This drone is equipped with a bottom camera and a front camera. The cameras each log their output to a topic. Additionally, message time stamps, the height sensor output, battery percentage, rotation velocity and acceleration are also logged to topics. While the drone can also be navigated using a PlayStation 3 controller, as shown in figure 17, showing a section of the `tum_simulation` package content structure, for an automated system, the drone should rather be addressed by publishing messages to the drone control topic (`/cmd_vel`) using the command line interface. For example by publishing messages of the class `Twist`, the drone can be navigated. With the command shown in listing 1, the drone is controlled to fly

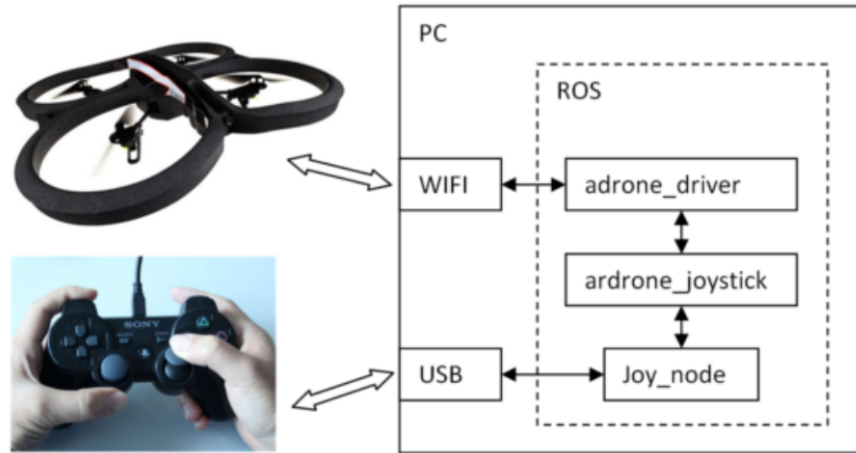


Figure 17: Tum simulator setup. Source: [http://wiki.ros.org/tum\\_simulator](http://wiki.ros.org/tum_simulator)

forward, as the linear translation vector points only in the x direction.

Listing 1: Drone navigation command

```

1      # navigate the drone forward
2      rostopic pub -r 10 /cmd_vel geometry_msgs/Twist '{'
3          linear: {x: 1.0, y: 0.0, z: 0.0}, angular: {x:
4              0.0,y: 0.0,z: 0.0}}'
```

In the next sections, the input and output topics of the drone are discussed.

## Input

### 1. /cmd\_vel

As mentioned, the node is subscribed to the /cmd\_vel topic. Whenever a valid navigation message is received, the drone reacts accordingly, if it can.

## Output

The drone has many sensors attached and more than thirty topics are logged to the system. However, here only the topics, that are of importance for the automation framework will be listed.

1. /ardrone/front/camera\_info

Over the /ardrone/front/camera\_info topic, the node publishes messages of the class CameraInfo. These messages include information about image dimension, timestamp and information about the camera specific values, described in section 2.1.2. In the case of the ardrone 2.0, the front camera generates images with 640x360 pixels and the intrinsic camera matrix is given by:

$$K = \begin{pmatrix} 374.6706070969281 & 0.0 & 320.5 \\ 0.0 & 374.6706070969281 & 180.5 \\ 0 & 0 & 1 \end{pmatrix}$$

2. /ardrone/front/image\_raw

The node publishes the actual output image data of the front camera in the /ardrone/front/image\_raw topic. The metadata of the camera are provided in the topic /ardrone/front/camera\_info described above.

3. /ardrone/navdata

Messages of the specially developed class Navdata are published to this topic by this node. These messages include information about battery percentage of the drone, state of the drone (e.g hovering, flying, init, landing...), pressure, temperature, wind, velocity and some more information. These messages are also timestamped.

4. /ardrone/takeoff

As the name of the topic suggests, the drone takes off, when empty messenges are published to the thred. How this looks exactly can be found in listing 2.1.2.

#### 5. /gazebo/model\_states

Gazebo provides the possibility to access the current pose of each model existing in a respective gazebo world. For example the ardronetestworld, that is displayed in figure 19, consists of the drone itself, several houses, a barrier etc.

Therefore, the /gazebo/model\_states topic publishes the list of the pose,  $x_i \in \text{SE}(3)$  of each model. However, in the ardronetestworld, only the drone is dynamic and important for this topic, all other models are static and therefore the pose will not change.

#### 6. /gazebo/collision

It is possible to implement a contact sensor to a gazebo model. However, currently the implementation has not yet been successful, as described in section 3.2.1.

### Real-life framework

For the real life framework, no gazebo simulation is running. Instead, a node processes the sensors of the drone within a node. The output topics of the drone are then limited to the drone sensors, as displayed in figure 16

#### 3.1.2 ORB-SLAM Node

The ORB-SLAM algorithm runs in a separate node. For the vocabulary file, needed for the bag of words approach, explained in section 1, the standard

vocabulary file provided by the authors are considered. For the virtual environment, it might be useful to provide a vocabulary file generated for this particular purpose, since in the simulation generated with the tum\_simulation, edges might be of different shape, e.g. particularly sharp.

The node publishes the pose  $x_i \in \text{SE}(3)$  and map points computed by the ORB-SLAM Algorithm. Because the original ORB ROS implementation didn't have an option for publishing data and projects, that implemented this functionality, these features had to be implemented.

## Input

1. /ardrone/front/image\_raw

This topic is explained in the upper section [3.1.1](#).

## Output

1. /orb/pose

This topic publishes messages of the class PoseStamped. This class includes a header, where the frame\_id and most importantly a timestamp can be provided. The pose is then given by x, y, and z position coordinates and the orientation is given with quaternions coordinates, that are discussed in section [2.1.2](#). The topic is published at a frequency of 30 Hz.

2. /orb/map\_points

This topic publishes messages of the class PointCloud and also runs at a frequency of 30 Hz. The class consists of a vector of points of the class Point32, all having x, y, and z coordinates containing 32 bit data.

### calculation

For the calculation of the pose and map points, the section [2.1.3](#) can be referred to.

#### 3.1.3 Alignment node

As mentioned in sectionasdfsdf gazebo provides the true positions of all models present in the gazebo world. Most importantly, this includes the pose of the drone. In order to transform the point cloud that is computed by the ORB-SLAM algorithm to the reference of the gazebo world, the estimated position by ORB-SLAM and the true position are again aligned with the method of Umeyama.

Therefore, this node computes the variables, that are needed for the transformation and outputs the resulting transformation matrix, translation vector and scale.

#### Input

1. /ardrone/true\_position

In order to align the trajectories, the true position of the drone is needed. While gazebo provides this data in the /gazebo/model\_states topic, the model positions do not include a timestamp. Because a timestamp is needed for the alignment in order to only align the matching positions, another node was created to add a timestamp to the gazebo output positions. This node subscribes to the /gazebo/model\_states topic and provides the data with a timestamp. To keep the time error, that results in reading in the topic data as small as possible, the node runs at an quite high frequency of 100 Hz.

Because the node is very simple only executes the task of stamping the true positions, it is not listed in this chapter.

## 2. /orb/pose

To align the ground truth position and the estimated position of ORB, the /orb/pose topic published by the ORB node described in section ?? is subscribed to by the node.

## Output

### 1. /scale

The node publishes the scale computed with the method of umeyama to the /scale topic.

### 2. /rotation\_matrix

The node publishes the rotation matrix as a flat numpy array computed with the method of umeyama to the /rotation\_matrix topic.

### 3. /translation

The node publishes the scale as a flat numpy array computed with the method of umeyama to the /translation topic.

## Real-life framework

In case, the framework is tested in real life, because the /ardrone/true\_position topic will be unavailable, the node subscribes to the /drone\_position\_init topic, published by the position estimation node instead.

## Computations

If all necessary nodes are up and running, the data logged to /orb/pose at 15Hz and to /ardrone/true\_position at 50 Hz is stored at two lists. This is done at a frequency of 10 Hz. Before aligning the points in the list, it is waited until 50 points are logged to each list. If only one list has reached the length of 50, new elements are stacked on top, while the oldest are removed.

Then, the lists are culled in a way, that the minimum and maximum of the timestamp align. This is done in order to save unnecessary resources in the following computations. transformation step. Since the lists now may be of different length because they origin from topics with different logging frequency, for the shorter list, for each element the element from the other list with the smallest time difference is matched. This assures that the points estimated by orb and from true position are measured at the same time.

Finally, the points are aligned by using the method of Umeyama, as described in section ?? and the scale, the rotation matrix and the translation vector are published to the topic.

These computational steps are processed in the main callback loop of the respective file for the node. The function of the main loop is shown in listing 2 in order to provide further clarification of the computation to the reader.

Listing 2: Main part of the scale estimation node

```

1 def update_trans_variables(self):
2     # return, if not enough points are available
3     # since no scale can be computed
4     if (len(self.est_pos_orb) < 50) or (len(self.
5         true_pos) < 50):
6         print("not enough data available, waiting
7             ...")

```

```
6         return
7
8     # return the scale if it already has been
9     # calculated
10    else:
11        # get minimum and maximum time for each
12        # queue to figure out,
13        # how many points can be considered for
14        # alignment. This is only done once!
15        min_orb = np.min([pose_oi.header.stamp.
16                           to_sec() for pose_oi in self.
17                           est_pos_orb])
18
19        max_orb = np.max([pose_oi.header.stamp.
20                           to_sec() for pose_oi in self.
21                           est_pos_orb])
22
23
24        min_true = np.min([point_oi.header.stamp.
25                           to_sec() for point_oi in self.true_pos
26                           ])
27
28        max_true = np.max([point_oi.header.stamp.
29                           to_sec() for point_oi in self.true_pos
30                           ])
31
32
33        thresh_min = np.max([min_orb, min_true])
34        thresh_max = np.min([max_true, max_orb])
35
36
37        # cut off the queues
38        orb_oi = [pose_oi for pose_oi in self.
39                  est_pos_orb if pose_oi.header.stamp.
40                  to_sec() > thresh_min]
```

```
23         true_oi = [pose_oi for pose_oi in self.
24                         true_pos if pose_oi.header.stamp.
25                         to_sec() > thresh_min]
26
27     # for the shorter remaining queue, get
28     # the matching point
29
30     if len(orb_oi) <= len(true_oi):
31
32         orb_oi_final = orb_oi
33         true_oi_final = []
34
35         for pose_oi in orb_oi:
36
37             diffs_oi = [np.abs(
38                             pose_oi.header.stamp.
39                             to_sec() - point_oi.
40                             header.stamp.to_sec())
41
42                 for point_oi in
43                 true_oi]
44
45             true_oi_final.append(
46                 true_oi[diffs_oi.index
47                         (min(diffs_oi))])
48
49
50     else:
51
52         true_oi_final = true_oi
53         orb_oi_final = []
54
55         for pose_oi in true_oi:
56
57             diffs_oi = [np.abs(
58                             pose_oi.header.stamp.
59                             to_sec() - point_oi.
60                             header.stamp.to_sec())
61
62                 for point_oi in
63                 orb_oi]
```

```
38                     true_oi_final.append(
39                         true_oi[diffs_oi.index
40                             (min(diffs_oi))])
41
42             # now do the alignment and compute the
43             # scale
44
45             x_orb = [pose_oi.pose.position.x for
46                     pose_oi in orb_oi_final]
47
48             y_orb = [pose_oi.pose.position.y for
49                     pose_oi in orb_oi_final]
50
51             z_orb = [pose_oi.pose.position.z for
52                     pose_oi in orb_oi_final]
53
54
55             x_true = [pose_oi.pose.position.x for
56                     pose_oi in true_oi_final]
57
58             y_true = [pose_oi.pose.position.y for
59                     pose_oi in true_oi_final]
60
61             z_true = [pose_oi.pose.position.z for
62                     pose_oi in true_oi_final]
63
64
65             orb_points = np.column_stack((x_orb,
66                                         y_orb, z_orb))
67
68             true_points = np.column_stack((x_true,
69                                         y_true, z_true))
70
71             s, R, t = align_umeyama(true_points,
72                                     orb_points)
73
74             R = R.reshape([9,])
75
76             # finally publish the computed scale,
77             # matrix and vector
```

```

55     if s>0:
56         self.scale_publisher.publish(
57             Float64(s))
58
59     if sum(np.isnan(R)) == 0:
60         self.rot_publisher.publish(R)
61
62     if sum(np.isnan(t)) == 0:
63         self.trans_publisher.publish(t)

```

### 3.1.4 Position Estimation Node

This node is only relevant for the real life framework. There, since no ground truth is available for the position of the drone, the position estimation node approximates the position of the drone based on the velocity on the drone and the latest position. ORB-SLAM, used in the visual monocular mode is as mentioned not able to extract the true scale of the environment. Estimating the true position enables us to also scale the computed point cloud by the ORB SLAM node to its true scale.

This method should be done in the initialization process, by only doing translational movements with the drone, such as a takeoff and a short forward movement. No rotations should be performed with the drone since the drone's navigation data, such as the velocity, uses the body-frame as reference frame. Thus doing rotations would result in an incorrect estimation of the position.

While relying on the information about the velocity of the drone, the drone needs to have inertial sensors attached. Having these IMU sensors, as the ARdrone 2.0 in the simulation does, also ORB SLAM would benefit from accuracy, since an integration in the algorithm is implemented. However, if drone does not have these sensors attached, this node can still be beneficial, since it is possible to manually publish messages to the /drone\_position\_init topic.

The initialization process could then be applied by manually flying the drone one meter up, and one meter forward and logging these points to the system. Then the automation process could be started.

Folling an overview over the input, output and computational functionality of the node.

## Input

The node subscribes to the following topics:

1. /ardrone/navdata

This topic is beeing published with the tum simulation node described in section 3.1.1. This node only uses the velocity vectors  $v_x \in \mathbb{R}, v_y \in \mathbb{R}, v_z \in \mathbb{R}$  given in the unit  $mms^{-1}$  included in the published navdata messages.

2. /drone\_position\_init

The drone also subscribes to the /drone\_position\_init topic, published by itself. This topic includes messages of the class PointStamped. This class includes the x, y and z coordinate of the point itself, and a timestamp. The node also needs the information from this topic, to read in the last position and update it based on the velocity, by doing the computations explained in the following section. The x y and z coordinates are transformed to meter.

## Output

The node publishes to the following topics:

1. /drone\_position\_init

This topic is explained in the upper section. The updated points are published in this topic.

## computation

As mentioned, the computation is made based on the current velocity

$$v_i = \begin{pmatrix} v_{i,x} \\ v_{i,y} \\ v_{i,z} \end{pmatrix} \in \mathbb{R}^3$$

and the latest position point

$$x_{i-1} = \begin{pmatrix} x_{i-1,x} \\ x_{i-1,y} \\ x_{i-1,z} \end{pmatrix} \in \mathbb{R}^3$$

. Also, the time difference in seconds to the last point is extracted, which is easy, since all objects from the class PointStamped can be timestamped. The difference is given by  $\Delta t_i = t_i - t_{i-1}$ . The updated position is the yielded by

$$x_i = x_{i-1} + \frac{\Delta t_i * v_i}{1000}$$

Dividing by 1000 yields the unit meter.

This recursive methodology is shown in figure 18

The implementation is easily deployed and the update function, that is running in the main loop can be seen in listing 3.

Listing 3: Main part of the position estimation node

```

1     def update_position(self):
2         # get velocity in x, y and z direction

```

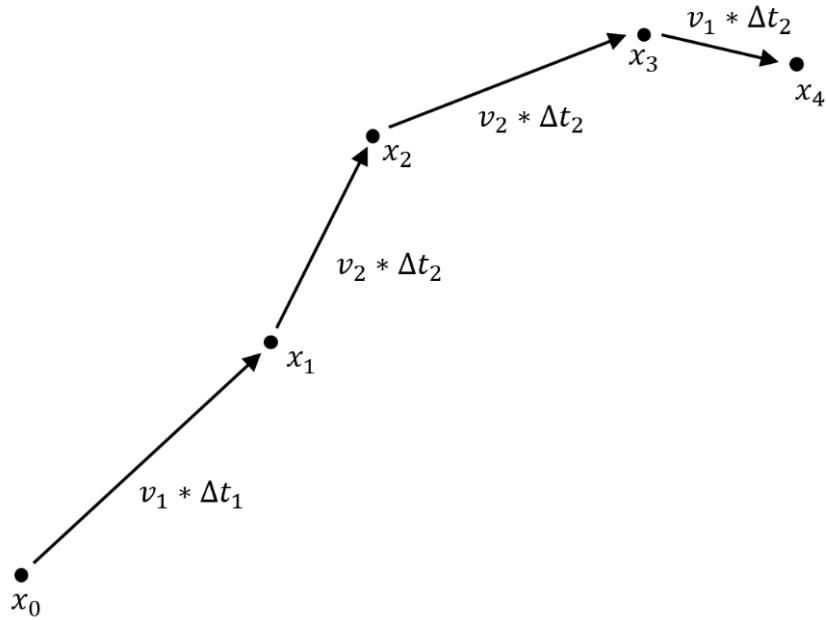


Figure 18: Calculation method for estimation the position in the initialization process in order to find the true scale.

```

3  x_vel = self.navdata.vz
4  y_vel = self.navdata.vy
5  z_vel = self.navdata.vz
6
7  if x_vel is not None and y_vel is not None and z_vel is
     not None:
8      # get time difference
9      curr_time = rospy.Time.now()
10     time_diff = (curr_time - self.position.header.
11                           stamp).to_sec()
12
13     # create the new point
14     new_point = PointStamped()
15     new_point.header.stamp = curr_time

```

```

15         new_point.header.frame_id = "init"
16
17     # update positions
18     new_point.point.x = self.position.point.x +
19         time_diff * x_vel / 1000
20     new_point.point.y = self.position.point.y +
21         time_diff * y_vel / 1000
22     new_point.point.z = self.position.point.z +
23         time_diff * z_vel / 1000
24
25     # publish
26     self.position_publisher.publish(new_point)
27     rospy.sleep(0.1)

```

### 3.1.5 Transformation and Restriction Node

This node processes the scale, rotation matrix and translation vector computed in the alignment node and transforms the ORB pose and the point cloud computed by ORB SLAM into the reference frame of the gazebo world. In addition, constraints are added to the searching space of the path finding algorithm by adding walls of points in the resulting point cloud of ORB.

These processes make sense for many reasons. On the one hand transforming the ORB\_SLAM output in the gazebo world creates the possibility to compare the estimated position of the ORB-SLAM-Algorithm to the ground truth position as it also has been done in the evaluation of the vSLAM algorithms. While it was not yet managed to extract the ground truth point cloud of the gazebo world, as described in section 3.2.1, it is technically possible, to also compare the ground truth point cloud to the generated one. On the other hand, it also enables users to track the path planned by the path planning algorithm relative

to its surrounding in the future.

The restriction of the searching space is useful, because the aim the path planning algorithm is to explore unseen areas in in the searching space. Obviously, since the path planning algorithm relies exclusively on the point cloud, unseen areas are then defined as areas, where no points are available. The gazebo world, displayed in figure 19, exceeds in unlimited space and therefore will cause the path finding algorithm to navigate in infinite space. Also the ground, sides and sky of the world have no texture, and will make it impossible to find features and therefore generate points for the ORB-SLAM-Algorithm. Unfortunately, as described in the issue section 3.2.1, no other world is yet available. Thus, adding points to limit the searching space is crucial. This is the reason why most navigation algorithm are constructed for indoor navigation.

## Input

1. /orb/map\_points

The ORB point cloud topic, described in section 3.1.2 is subscribed to by the node.

2. /orb/pose

Since also the pose is transformed in the gazebo reference frame, the /orb/pose topic is also used as input.

## Output

1. /pointcloud\_transformed

The node publishes data to the topic /pointcloud\_transformed with messages of the class PointCloud. Therefore, the point cloud contains the transformed point cloud of ORB SLAM and the points, that are inserted

to limit the searching space of the flight path finding algorithm. The exact computations are shown in section below.

## 2. /pose\_transformed

Also the orb pose is transformed and published in the /pose\_transformed topic. The timestamp for the transformed pose is taken from the original pose calculated by ORB, since the alignment process relies on the timestamp, when the pose was computed.

### computation

First, all points  $p_i$  in the point cloud and the estimated positions are transformed with the rotation matrix  $R$ , scale  $s$  and transformation vector  $t$  received from the above described topics. The resulting points are therefore computed by:

$$p'_i = sRp_i + t$$

Then, the restriction points are added to the point cloud. The ground plane of the gazebo world has a size of 100x100, but only the center is filled with objects (models). The middle of the plane lies in the exact origin of the gazebo world. The goal is to restrict the search space of the path planning algorithm to the hull of a cuboid with 15m height, 60m length and width. The cuboid is therefore given by:

$$\Omega = \{(x, y, z) \in \mathbb{R} : x \in [-30, 30] \wedge y \in [-30, 30] \wedge z \in [-30, 30]\}$$

Then, 10000 points for each side of the hull of  $\Omega$  are added to the generated point cloud by ORB, after it was transformed. This can simply be achieved

in three consecutively for loops. This is shown in listing 4 for the upper and lower restrictions. These loops are run for the sides respectively.

Listing 4: Adding upper and lower restrictions to point cloud.

```

1
2 # bottom and top
3 for x_oi in np.linspace(-30, 30, 100):
4     for y_oi in np.linspace(-30, 30, 100):
5         for z_oi in [0, 15]:
6             p_out = Point32()
7             p_out.x = x_oi
8             p_out.y = y_oi
9             p_out.z = z_oi
10            pq.points.append(p_out)

```

Note that for the point cloud the coordinates are only stored in 32 bit to save resources, since the point cloud can contain ten thousands of data-points. In order not to overload the system, the transformation node runs on a frequency of only 5Hz, which results in smooth computation.

### 3.1.6 Flight Path Planning Node

The flight path planning node is in charge of autonomously navigating the drone. This should be done without colliding with any obstacles. On the other hand, since the goal is to explore the environment, the algorithm should always thrive to visit new areas in order to generate new map points.

While the computation of this node is not yet implemented and is not part of this work, the desired input and output can be cleanly defined. Also approaches currently used in for path planning approaches in active SLAM-application are described in the computation section.

## Input

1. /pointcloud\_transformed

This topic is explained in the upper section.

2. /pose\_transformed

This topic is explained in the upper section.

3. /pose\_transformed

This topic is explained in the upper section.

4. /gazebo/collision

For the simulated framework, the node also may subscribe to the /gazebo/collision topic. This enables users to penalize the algorithm in the training process, in case the obstacle avoidance did not succeed.

## Output

1. /cmd\_vel

The node should publish navigation commands to /cmd\_vel, as shown in example 1.

## Computation approaches

The path planning task for autonomous exploration is also related to visual servoing, which is a technique to control a robot, by directly feeding it visual information. However, for most of these techniques, the observation target has to be predefined and is also assumed to always be in the field of view.

In most visual servoing methods, feedback signals for the servoing controller are estimated by means of multiple-view geometry

assuming the target scene being always within the camera field of view (FOV) [18].

While the research in the field of automated exploration algorithms is still in its early years [5] and will probably be mainly performed in simulated environment in the near future [23], some frameworks on tackling the task already exist [5], [23] [35] [19].

In this section, approaches, that the path flying node could be based on are explained.

Typically, it consists of three stages [8]: (i) the identification of all possible locations to explore (ideally infinite), (ii) the computation of the utility or reward generated by the actions that would take the robot from its current position to each of those locations and (iii) the selection and execution of the optimal action [23].

A general framework for decision making processes within a certain environment was introduced with the Partially Observable Markov Decision Processes (POMDP) framework. The active SLAM problem can be formally defined within this framework. The POMDP framework relies on seven components [? ], listed below.

- Set of States  $S$
- Set of Actions  $A$
- Set of conditional transition probabilities  $T : \mathbb{P}(s'|s, a)$
- Reward function  $R : A, S \rightarrow \mathbb{R}$
- Set of beliefs  $b$
- Set of observations  $Z$

- Set of conditional observation probabilities  $O : \mathbb{P}(z|s)$

$S$  defines all possible states, the drone can be in. In our case, a state is defined in the orientation of the drone, the position of the drone and the collision sensor output. All possible states are contained in a combination of all possible poses  $SE(3)$ , while the respective translational vector has to be in the cuboid  $\Omega$  defined in section ??, and all possible collision states, which is equal to  $\{0, 1\}$ . The current state can be extracted by the subscribed topics of this node.

All possible actions are all possible control commands, that can be published to the /cmd topic. This includes rotational and translational maneuvers. A possible command in order to make the drone fly forward?? can be seen in listing ??.

The function  $T$  returns the probability, a desired state  $s'$  is accessed by taking an action  $a$  in the state  $s$ .

The reward function  $R$  returns a reward in the form of a real number for an action taken in a state. In our case, the reward function should be defined in a way, that actions, resulting in a great amount of new observed points should be rewarded greatly, while actions, that result in no new observed features or even a crash, should be given little, no or negative reward. Defining a good reward function is crucial in order for the algorithm to work properly. An example reward function for our case could look like this:

$$R(a, s) = \begin{cases} n & \text{for } n \text{ newly explored points by ORB-SLAM, after action } a \text{ in state } s \\ -15 & \text{if tracking is lost, after action } a \text{ in state } s \\ -30 & \text{if the drone collided, after action } a \text{ in state } s \end{cases}$$

The belief  $b$  defines the probability for every state, that the drone actually is in this state. Therefore all probabilities should add up to one. Not all algorithms require  $b$  [30].

The set of observations  $Z$  equals the current pose and and current map points. Finally,  $O$  returns the probability to make an observation  $z$  while being in the state  $s$ . The POMDP is looping the follwing steps: Take action based on belief state, take observations and update belief state. The goal of the POMDP framework to create a policy  $\pi$  that maps states into actions. This policy is optimal, when it maximizes the sum of exprected reward in the future. There are several methods to find a policy, given the above components. In this paper, three of those methods are discussed.

### 1. Reinforcement learning

Unlike most other machine learning algorithm, reinforcement learning does not require training data for learning behavior. The learning mechanism is soly based on the reward, that is given for an action. Q-learning approaches don't need the definition of  $O$  and  $T$ . This is why Q-learning is defined as a model-free machine learning process [23].

Q-learning is a method of reinforcement learning. Approaches on applying it for robot navigation exist [35][23][19]. Q-learning approaches don't need the definition of  $O$  and  $T$ . Instead, Q-learning defines a recursive function  $Q$  that is based on the accumulated reward for a series of actions. If a drone is in a state  $s$ , the action  $a'$  is performed, that maximizes  $Q$  [19].

$$a' = \pi(s) = \arg \max_a Q(s, a)$$

At each iteration, the value of  $Q(s, a)$  is updated with the following term:

$$\Delta Q(s, a) = \alpha(R(a, s) + \gamma \arg \max_{a'} Q(s', a') - Q(s, a)). \quad (3.1)$$

$\gamma$  is called the discount factor and is a value between 0 and 1 and defines, how much weight is given to the reward for steps that are further away from the current one. For example, if  $\gamma = 0.8$ , the third term of the cummulated sum is only weihted with  $0.8^3 = 0.512$ . Thus, the more

reliable the algorithm and the chosen reward function is, the higher  $\gamma$  can be chosen, and therefore the better the algorithm plans the navigation into the future.

The exact computational steps are shown in algorithm 1. First, the learning rate  $\alpha$ , and the discount function  $\gamma$  have to be predefined. One possibility to find the optimal values for  $\alpha$  and  $\gamma$  is to perform a grid search. For the grid search and for the Q-learning algorithm also a mapping function has to be designed, that maps the point cloud to a value that determines, how far the target exploration process has proceeded. This function could for example be examining the point clouds distribution within the searching space.

Also, a number of episodes to train the models has to be defined. This is equal to the number of runs that are performed until the agent, in our case the drone, gets to a terminal state. A terminal state is a state, where the agent is finished. In our case, that would be equal to the state, where the drone collided, or a termination constrain has been hit when the exploration task has been successfully finished. This termination constrain could for example be a reached threshold of the previously defined mapping function.

Then in the algorithms while loop, in each episode, the algorithm iterates, by updating the Q-table, until a terminal state is reached. The Q-table is a matrix, that consists of all possible actions as columns and all possible states as rows. The Q-table is updated after every action by using the

update rule stated in equation 3.1.

**Data:** Parameters:  $\alpha \in (0, 1]$ ,  $\gamma \in (0, 1]$ , Initialize Q-table with arbitrary Q-values

```

for episode  $\leftarrow 1$  to max episode do
    Percieve  $s_t$  ;
    while  $s_t$  not terminal do
        select  $a_t = \pi(s_t)$ ;
        Take  $a_t$ , Get  $R(a_t, s_t)$ , percieve  $s_{t+1}$ ;
        if  $s_{t+1}$  is terminal then
             $Q_t \leftarrow R(a_t, s_t)$  ;
        else
             $Q_t \leftarrow R(a_t, s_t) + \gamma \arg \max_{a'} Q(s_{t+1}, a')$ 
        end
         $Q(s_t, a_t) \leftarrow (1 - \alpha)Q(s_t, a_t) + \alpha Q_t$  ;
         $s_t \leftarrow s_{t+1}$  ;
    end
end
```

**Algorithm 1:** Q-learning algorithm. Source: [23]

In the recent years, successes were made in the applyance of deep reinforcement learning algorithms for robotic navigation and exploration [23] [35]. These approaches don't analytically compute the output of  $Q$  but rather a Deep Neural Network is created in order to predict the output. Since for algorithm 1, in each step each action is calculated recursivly, the computation requires a lot of computational resouces. By approximating the function  $Q$ , this is avoided.

Also research has shown, that the trained models also yield good performance for environments, where they were not trained and have no a priori knowlege.

The results of [23] also shows, that the trajectory accuracy can be increased be autonomously navigating the drone.

D3QN results are the most remarkable in the first environment, as it outperforms the reward that a human would obtain by manually controlling the robot (approx. 350). In the second environment both DDQN and D3QN show a good behavior. Despite DDQN have higher SR (and mean steps, thus), the higher mean reward obtained by D3QN proves the generation of more optimal trajectories: smoother movements and less spins. [23]

D3QN is also a path planning algorithm based on deep reinforcement learning proposed by Wen et al in 2020 in their work Path planning for active SLAM based on deep reinforcement learning under unknown environments [35].

## 2. Other approaches

Aside from the above-discussed reinforcement learning methods, other approaches to tackle the path planning task exist.

Back in 2006, Leung et al published their work Active SLAM using Model Predictive Control and Attractor based Exploration [17].

In their work Active SLAM and Exploration with Particle Filters Using Kullback-Leibler Divergence [4], Carlone et al suggested....

## 3.2 Current setup

In figure [? ] the simulated environment with gazebo can be found in figure a. Here, the drone (in black) is flying in front of the building. The output of the front camera is shown in figure b. In figure c, the ORB-SLAM-Algorithm was applied to the output of the front camera. Green dots represent the finding of a ORB-features.

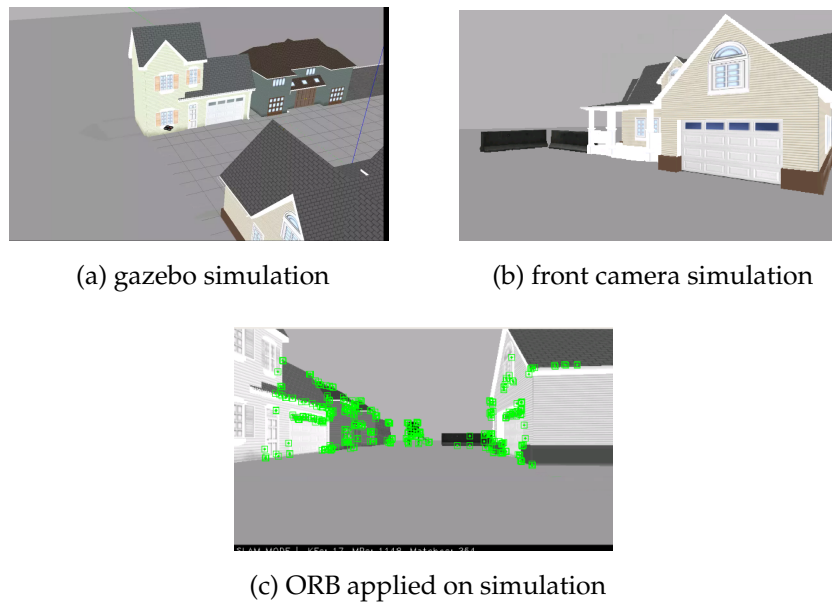


Figure 19: The drone in a gazebo simulation in a), the output of the front camera of the drone in b) and the ORB-SLAM algorithm applied on the front camera output in with the detected ORB features marked green c).

Currently the framework is set up in an environment provided by theconstructsim.com. This platform is enabling ROS-developers to program in preconfigured ROS-environments. The environment comes with the possibility to open terminal consols, a file management system, a gazebo simulator, that automatically detects, when a gazebo simulation is running. Also, you have a graphical interface for other graphical applications, such as the viewer of ORB-SLAM. The current environments is set up with ROS kinetic and Ubuntu 16.04.6 LTS (Xenial). The tum\_simulator, ORB-SLAM and all of their dependencies are already installed. The provided machine consists of 16 processing kernels and contains a total RAM space of 29 GB. The hard drive offers 92 GB of available space. However, theconstructsim.com limits each user to 8 hours daily on the platform.

The project is publicly available under the name tum simulator test.

Listing 5: Launching the simulated environment

```
1
2 # launch the gazebo simulation
3 roslaunch cvg_sim_gazebo ardrone_testworld.launch
4
5 # launch ORB-SLAM
6 rosrun ORB_SLAM2 Mono ${PATH_TO_VOCABULARY} ${
7     PATH_TO_SETTINGS_FILE}
8
9 # start the scale estimation node
10 rosrun auto_explorer scale_updater.py
11
12 # start the position estimation node
13 rosrun auto_explorer position_updater.py
14
15 # takeoff with drone
16 rostopic pub -1 /ardrone/takeoff std_msgs/Empty
17
18 # Then start flight path planner algorithm
```

In listing 5 the commands for launching the gazebo simulation, ORB-SLAM and the drone are displayed. After launching those applications, only the path planning algorithm based on the resulting point cloud is missing. However, multiple solutions for such algorithms exist [11], applying it on the system is not part of this paper and will be done in further research.

### 3.2.1 Known Issues

1. Only one world available

For the tum\_simulator it might be useful to continue the automation process in another simulated world. This is because the current world named

ardrone\_testworld doesn't contain any contours or relief on the ground, and sky, as shown in figure ???. Since the ORB-SLAM algorithm is looking for features such as edges and changes in pixel intensities, it will not find any on the ground, which will result in no points available in this area for the resulting point cloud. While there are many worlds available in the tum\_simulator package, since the package is originally not made for ROS kinetic, these worlds will not compile and running the command to start one of those worlds, as shown in listing 6 will result in the following error:

```
ERROR: cannot launch node of type [gazebo/spawn_model]: gazebo.
```

So far, no solution has been detected, but one possible workaround would either be to build another world from scratch. Another possible solution would be to add flying constraints to the path planning algorithms, that limits the environments on a predefined volume. This solution is implemented by the bla bla node, described in section ??, which restricts points to the point cloud.

Listing 6: Launching different world

```
1  
2 # launch different world named land_station1  
3 roslaunch cvg_sim_gazebo land_station1.launch
```

## 2. No ground truth point cloud

While the pose and position of the models in the gazebo world, such as the drone itself, the houses and other objects, are known, it was not yet possible to convert these objects into pointclouds.

This refuses the possibility to compare the evaluated points by the ORB algorithm in the ROS setup, to their true position. Users of the setup now have to solely rely on the results of evaluation described in section ??.

## 3. Collision sensor not working

Gazebo provides the possibility to attach collision sensors to models existing in the world. These sensors can simply be defined in the respective XML file of the model. However, even after the implementation and no error message, the respective topic, where the data should be published, does not appear when calling the rostopic list command. So far, no solution could be found.

## **4. Summary**

# Bibliography

- [1] W. Burgard et al. Introduction to mobile robotics.
- [2] M. Burri. The euroc micro aerial vehicle datasets. *The International Journal of Robotics Research*, 2016.
- [3] C. Campos et al. Orb-slam3: An accurate open-source library for visual, visual-inertial and multi-map slam. 2021.
- [4] L. Carlone et al. Active slam and exploration with particle filters using kullback-leibler divergence. 2014.
- [5] S. Chaves et al. Opportunistic sampling-based planning for active visual slam. 2013.
- [6] A. J. Davison, I. D. Reid, N. D. Molton, and O. Stasse. Monoslam: Real-time single camera slam. *IEEE Transactions on Pattern Analysis and Machine Intelligence*, 29(6):1052–1067, 2007.
- [7] C. Debeunne et al. A review of visual-lidar fusion based simultaneous localization and mapping. 2020.
- [8] H. DURRANT-WHYTE et al. Simultaneous localization and mapping: Part i. 2006.
- [9] E. Eade. Lie groups for computer vision. 2002.
- [10] J. Engel et al. Direct sparse odometry. 2016.

- [11] A. Gasparetto et al. Path planning and trajectory planning algorithms: a general overview. 2015.
- [12] B. Hiebert-Treuer. An introduction to robot slam (simultaneous localization and mapping). 2015.
- [13] A. Huletski et al. Evaluation of modern visual slam methods. 2016.
- [14] G. Klein et al. Parallel tracking and mapping for small ar workspaces. 2007.
- [15] R. Kummerle et al. On measuring the accuracy of slam algorithms.
- [16] C. Leung, S. Huang, and G. Dissanayake. Active slam using model predictive control and attractor based exploration. pages 5026 – 5031, 11 2006.
- [17] C. Leung, S. Huang, and G. Dissanayake. Active slam using model predictive control and attractor based exploration. pages 5026 – 5031, 11 2006.
- [18] C. Li, X. Zhang, H. Gao, R. Wang, and Y. Fang. Bridging the gap between visual servoing and visual slam: A novel integrated interactive framework. *IEEE Transactions on Automation Science and Engineering*, pages 1–11, 2021.
- [19] E. Lopez et al. An active slam approach for autonomous navigation of nonholonomic vehicles. 2013.
- [20] E. Mingachev, R. Lavrenov, E. Magid, and M. Svinin. *Comparative Analysis of Monocular SLAM Algorithms Using TUM and EuRoC Benchmarks*, pages 343–355. 09 2020.
- [21] R. Mur-Artal. Orb-slam: a versatile and accurate monocular slam system. *IEEE TRANSACTIONS ON ROBOTICS*, 2015.

- [22] G. Pepe, M. Satler, and P. Tripicchio. Autonomous exploration of indoor environments with a micro-aerial vehicle. 11 2015.
- [23] J. Placed et al. Aa deep reinforcement learning approach for active slam. 2020.
- [24] O. Roesler and V. P. Ravindranath. Evaluation of slam algorithms for highly dynamic environments. 2020.
- [25] E. Rublee. Orb: an efficient alternative to sift or surf. 2012.
- [26] C. Sampedro et al. A fully-autonomous aerial robot for search and rescue applications in indoor environments using learning-based techniques. 2019.
- [27] R. Smith et al. On the representation and estimation of spatial uncertainty. *The International Journal of Robotics Research*, 1986.
- [28] H. Strasdat. Visual slam: Why filter? *Image and Vision Computing*, 2000.
- [29] T. Taketomi et al. Visual slam algorithms: a survey from 2010 to 2016. *IPSJ Transactions on Computer Vision and Applications*, 2017.
- [30] V. Thomas et al. Monte carlo information-oriented planning (revised version). 2020.
- [31] B. Triggs. Bundle adjustment – a modern synthesis. *International Workshop on Vision Algorithms*, 2000.
- [32] S. Umeyama. Least-squares estimation of transformation parameters between two point patterns. *IEEE Trans. Pattern Anal. Mach. Intell.*, 1991.
- [33] J. Wang et al. Mapping quality evaluation of monocular slam solutions for micro aerial vehicals. 2019.
- [34] S. Weiss, D. Scaramuzza, and R. Siegwart. Monocular-slam-based navigation for autonomous micro helicopters in gps-denied environments. *J. Field Robotics*, 28:854–874, 11 2011.

- [35] S. Wen et al. Path planning for active slam based on deep reinforcement learning under unknown environments. 2020.
- [36] Z. Zhang et al. A tutorial on quantitative trajectory evaluation for visual(-inertial) odometry. 2009.
- [37] J. Zubizarreta et al. Direct sparse mapping. 2019.